Research Square

Preprints are preliminary reports that have not undergone peer review.
They should not be considered conclusive, used to inform clinical practice,
or referenced by the media as validated information.

Multi-Source Geotechnical Characterization and Axial Bearing Capacity of Cast-in-Place Bored Piles in Alluvial Soils

Ahmad Alyaqoobi
University of Shatrah
Kumail Al-Khafaji
kumailr@shu.edu.iq
University of Shatrah
Aws Yaseen
University of Shatrah
Ahmed Jawad
University of Shatrah
Ahmed Abdulrasool
University of Technology
Husam Ahmed
General company of electrical energy distribution, southern region, ministry of Electricity

Research Article

Keywords: axial bearing capacity, cross-hole seismic testing, shear-wave velocity, standard penetration test, parameter reconciliation

Posted Date: November 6th, 2026

DOI: https://doi.org/10.21203/rs.3.rs-11391374/v1

License: This work is licensed under a Creative Commons Attribution 4.0 International License.
Read Full License

Additional Declarations: No competing interests reported.

Article

Multi-Source Geotechnical Characterization and Axial Bearing Capacity of Cast-in-Place Bored Piles in Alluvial Soils

Ahmad Alyaqoobi [1], Kumail Al-Khafaji [*], Aws Yaseen [1], Ahmed Jawad [1], Ahmed Abdulrasool [2], Husam Ahmed [3]

[1] Civil Engineering Department, University of Shatrah, Dhi-Qar, Iraq; ahmedmahdi@shu.edu.iq
[2] Civil Engineering Department, University of Technology, Baghdad, Iraq; ahmed.s.abdulrasool@uotechnology.edu.iq
[3] General company of electrical energy distribution, southern region, ministry of Electricity, Dhi-Qar, Iraq; husam1312@gmail.com
* Correspondence: kumailr@shu.edu.iq

Abstract

Axial design of bored piles requires combining measurements that sample different soil volumes, strain regimes, and failure processes. This paper compares SPT resistance, CPTU soundings, cross-hole seismic profiles, laboratory strength data, and static compression tests of eight 800 mm diameter bored piles (18.2-22.2 m long) at the Dhi-Qar Combined Cycle Power Plant, southern Iraq. SPT, Vs, and borehole descriptions all identify a common stiffness transition at 13-16 m, with median SPT N rising from 12 to 56 and mean Vs from 217 to 517 m/s. However, the apparent SPT-Vs correlation (pooled r = 0.835) is largely a depth artifact: both variables are strongly depth-dependent, and depth-adjusted descriptive correlations fall to r = 0.45 after linear depth adjustment and r = 0.39 after within-profile demeaning. Because the observations are nested within four profiles, these correlations are descriptive rather than independent inferential tests. Penetration-implied undrained strength is 2.40-4.21 times laboratory strength; known biases explain only about half of this gap. Small-strain stiffness ratios (6,100-6,800) confirm that seismic stiffness cannot substitute for strength parameters. Proof tests at twice service load produced head movements of 2.50-7.53 mm (0.31-0.94% of D), of which 13-70% is elastic pile shortening rather than ground deformation. The eight-pile dataset is too small for reliable resistance-factor calibration. The study's contribution is methodological: multiple sources can agree on stratigraphy while disagreeing on design parameters, and reconciliation requires explicit treatment of spatial support, strain regime, and transformation uncertainty.

Keywords: axial bearing capacity; cross-hole seismic testing; shear-wave velocity; standard penetration test; parameter reconciliation.

1. Introduction

The axial design of a cast-in-place pile is, at its core, an inverse problem. The designer must infer the three-dimensional load-transfer behavior from a limited and incomplete set of measurements taken from borehole logs, penetration tests, geophysical measurements, construction records, and field load tests. All of these types of evidence are useful, but none of them samples the soil-pile system at the same strain level or over the same volume: laboratory tests examine small specimens, SPT and CPT/CPTU tests measure how resistant the soil is to penetration, cross-hole seismic tests record how small-strain

Received: date
Revised: date
Accepted: date
Published: date

Copyright: © 2026 by the authors. Submitted for possible open access publication under the terms and conditions of the Creative Commons Attribution (CC BY) license.

waves travel through the ground, and static pile tests show how the structure and foundation react to load.

Static axial compression testing, following [1], remains the most direct field means of relating an applied axial load to the movement of a deep foundation element [1]. But a proof test that stops at some prescribed multiple of the service load, without ever reaching a displacement-based failure criterion, only establishes a verified lower bound on resistance; it is not an observed ultimate capacity. Extrapolation methods help here, but their output is model-dependent and should not be reported as a measured failure load.

Cross-hole seismic testing gives an independent line of evidence at strains far below those of conventional strength testing. The method of determining the velocity of compressional and shear waves in low-strain conditions is outlined in ASTM D4428/D4428M (ASTM International, 2025). The relationship between measured shear-wave velocity and maximal small-strain shear modulus is given by Eq. $Gmax = \rho Vs^2$, where ϱ is soil mass density. [2] separates small-strain stiffness from ultimate strength in foundation applications of shear-wave velocity. That distinction governs the use made of Vs here: seismic velocity verifies stiffness profiles and locates stratigraphic transitions, and does not stand in for the parameters that govern pile resistance.

Cone penetration testing provides high-resolution in-situ profiling. The original project documentation includes normalized soil behavior type (SBTn) classifications and CPT/CPTU data for cone resistance, sleeve friction and pore-water pressure based on the Robertson framework [3]. These data help track the lateral continuity of shallow and intermediate strata between boreholes. Their value at pile toe depth depends on two things: how deep the sounding goes relative to the toe, and how near it sits to the pile under consideration.

Published work supports the combination of sources of geotechnical information, but warns against the naive use of broad empirical transformations. [4] reviewed the correlations of Vs-SPT and observed that they are sensitive to the geological environment, stress state, soil type, saturation and regional calibration. [5] showed that seismic velocity may be used to complement traditional indicators of pile capacity and cross-hole seismic testing has been utilized in Iraq to identify depth-dependent changes in stiffness and bearing conditions [6], [7] What is lacking is an interpretative framework that illustrates the concordance or discordance of independent measurements and the extent to which this should alter confidence in the resultant capacity estimations.

The present study is consequently concerned with the reconciliation of multiple approaches of parameter estimate as part of the design process itself. [8] proposed a comparison of many methodologies for forecasting soil characteristics, and [9] revealed that geotechnical parameters had both intrinsic spatial variability and transformation uncertainty. Both sources of uncertainty are important when combined with laboratory strength, penetration resistance and seismic stiffness. Where there is agreement trust in the ground model is increased. Where there is disagreement it may suggest scale effects, incompatible strain regimes, sample disturbance or a transformation that is not here applicable. Thus, this article evaluates convergence and inconsistency before comparing the analytical pile resistance to the observed field response.

The bored-pile literature makes the same point: no single indicator can adequately represent axial performance. [10] separated the displacement of the pile head into two parts, elastic pile compression and ground deformation. Regulating variables are considered by [11] and [12] and include shaft-interface conditions, resistance mobilization and building method. [13] advocated the use of design frameworks combining mechanics-based analysis and site-specific empirical calibration. [14] showed that the shaft resistance depends on soil type, stress history and installation effects. The relationship between predicted capacity and measured load settlement response in cast-in-place piles can be affected by shaft roughness, excavation stability, groundwater conditions and foundation cleanliness. At El Alamein, Egypt, [15] conducted a field experiment on long, large-diameter drilled piles in interbedded geomaterials. Their program is the closest recent benchmark to this one. Their database recorded 44 static and dynamic compression tests on piles with diameters ranging from 800 mm to 1,200 mm.

At nearly twice the design load, settlement remained below 1.6% of the pile diameter. The 800 mm piles, in particular, settled by approximately 7 mm (approximately 1% of D) without reaching an ultimate failure condition. Elsakhawy et al. regarded their piles primarily as friction piles and proposed that measured field response should be used to calibrate analytical design assumptions. Despite the fundamental distinction between the saturated alluvial clay-sand profile at Dhi-Qar and the El Alamein ground (intermediate geomaterials and weak limestone), the shared pile diameter, proof-load level, and normalized movement make it a usable external benchmark.

This study utilized the Dhi-Qar Combined Cycle Power Plant database to address that need, drawing on the compiled static load-test and capacity data together with the original investigation packages for TP1-TP8. The objectives of the study are as follows: (i) to confirm the source-data architecture and spatial offsets between boreholes, cone penetration soundings, and cross-hole profiles; (ii) to quantify laboratory, penetration, and seismic depth trends; (iii) to cross-check the laboratory undrained strength against the strength implied by the project design-basis penetration correlation; (iv) to evaluate the strain-scale compatibility of laboratory strength and cross-hole small-strain stiffness; and (v) to quantify the bias between the analytical axial capacity and the load-test-derived capacity, and its implication for resistance-factor selection.

2. Site and Investigation Program

The study site is the Dhi-Qar Combined Cycle Power Plant in southern Iraq. The investigation records date primarily from March-April 2017 and comprise borehole logs, laboratory summaries, SPT records, CPT/CPTU sounding plots, cross-hole seismic tables, and subsequent pile-load-test data. The piles considered in the main comparison are 0.8 m diameter cast-in-place bored piles. TP-1 and TP-6 are 18.2 m long with a service load of 810 kN; TP-2, TP-3, TP-4, TP-5, TP-7, and TP-8 are 22.2 m long with a service load of 1450 kN. The static tests were generally taken to approximately 200% of service load, with TP-A providing an additional higher-load cycle in the compiled test database (Dhi-Qar Combined Cycle Power Plant, 2017). The project test-pile location plan is reproduced in Plate 1 and shows the spatial distribution of TP1-TP8 across the plant site.

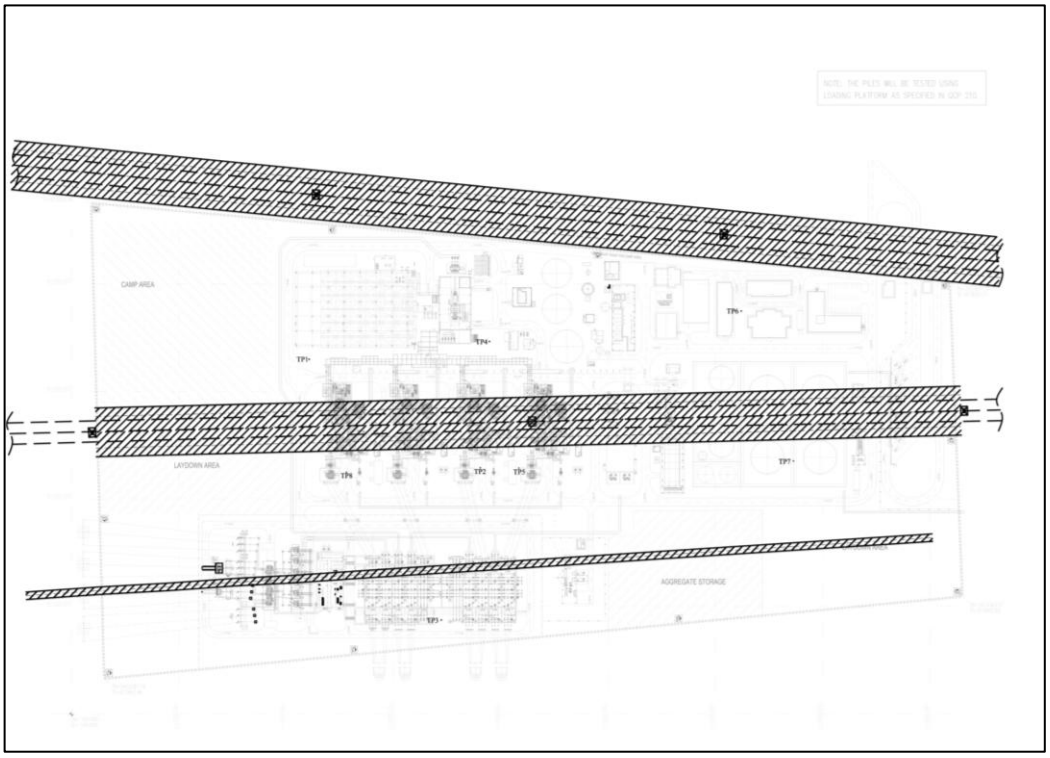


Plate 1 Project test-pile location plan showing TP1-TP8 and the specified test loads at the Dhi-Qar Combined Cycle Power Plant.

2.1 Original-data verification and spatial arrangement

The original TP1-TP8 source packages define the investigation database. Each pile package contains a conventional borehole/laboratory record and a CPT/CPTU sounding. Five packages also contain cross-hole information, but some cross-hole tables are duplicated between packages. After removing duplicates, four unique seismic profiles remain: CHT-1, CHT-3, CHT-4, and CHT-5. CHT-1 is contained in the TP-8 package. It provides a fourth unique profile and extends the SPT-seismic consistency analysis to BH01/CHT-1.

Table 1 Verified investigation coverage from the original TP1-TP8 source packages (Dhi-Qar Combined Cycle Power Plant, 2017).

Pile	BH	GWT (m)	Pile L / service load	CPT depth (m)	BH-CPT offset (m)	Cross-hole content
TP-1	BH51	1.80	18.2 / 810	12.80	60.2	CHT-5 (full dynamic)
TP-2	BH15	2.00	22.2 / 1450	13.20	24.6	CHT-3 (full dynamic)
TP-3	BH85	1.85	22.2 / 1450	11.24	20.1	None
TP-4	BH58	1.85	22.2 / 1450	14.18	45.1	CHT-5 velocity + duplicated CHT-3
TP-5	BH22	2.40	22.2 / 1450	12.00	24.7	CHT-4 (full dynamic)
TP-6	BH32	1.60	18.2 / 810	12.14	132.3	None
TP-7	BH35	1.90	22.2 / 1450	11.72	74.8	None
TP-8	BH01	1.80	22.2 / 1450	13.10	24.6	CHT-1 (full) + duplicated CHT-4 velocity

The borehole-CPT plan offsets calculated from the reported coordinates range from 20.1 to 132.3 m (median approximately 34.9 m). These offsets are not errors; they reflect the project-scale investigation layout. They are nevertheless important because a CPT trace should not be interpreted as a perfectly collocated duplicate of a borehole profile. Cross-hole coordinates were not provided in the source tables, so direct cross-hole-to-pile

distances cannot be reconstructed from the available records. Cross-hole IDs in Table 1 therefore describe source-package content rather than guaranteed collocation.

2.2 Laboratory tests

The laboratory dataset contains a wide range of index, strength, compressibility, and chemical properties, such as Atterberg limits, natural water content, dry density, specific gravity, consolidation indices, swelling pressure, and the percentage passing the No. 200 sieve. Unconfined compression, triaxial, or direct-shear tests were used to determine strength characteristics, and selected chemical indications were also provided.

A number of fields in the laboratory records were simply left blank, and we considered them missing rather than zero, because assigning a zero would have produced artificial bias in the data. The results that are currently available suggest that the deposits are fine-grained and have medium to moderate plasticity. The project records do not, however, report a complete or consistent set of clay parameters across the full investigation profile.

Table 2 The principal ranges observable in the original laboratory summaries are as follows (Dhi-Qar Combined Cycle Power Plant, 2017).

Property	Reported range	Interpretive significance
Liquid limit, LL (%)	38-78	Wide plasticity range across silty-clay strata
Plasticity index, PI (%)	18-45	Moderate to high plasticity
Natural water content (%)	19.8-31.9	Consistent with saturated/near-saturated fine-grained deposits
Dry density (kN/m³)	12.9-16.3	Substantial density variation between samples
Specific gravity	2.66-2.73	Relatively consistent mineral-soil range
Unconfined compressive strength (kPa)	68-118	Reported for selected undisturbed samples
Initial void ratio, e_0	0.743-0.934	Compressibility varies materially among sampled clays.
Pre-consolidation pressure, Pc (kPa)	95-190	Indicates variable stress history
Compression index, Cc	0.17-0.32	Moderate compressibility where reported
Recompression index, Cr	0.029-0.061	Reported consolidation rebound range
Swelling pressure (kPa)	6-28	Low-to-moderate reported swelling pressures
Passing No. 200 (%)	23.6-99.1	Confirms alternation from fines-dominated soils to sandier horizons

Most laboratory results are derived from the top 10 m or so, so assessments at greater depths are more dependent on borehole descriptions and penetration resistance. This is important for pile capacity. The 18.2-22.2 m piles extend well below the depths with the greatest concentration of undisturbed lab data.

2.3 SPT and CPT/CPTU

SPT N-values are presented in all eight borehole logs. The original reports lack metadata on hammer energy, borehole diameter, rod length, and sampler correction, so the N-values reported remain the reported N-values in this study and are not relabeled as a rigorously corrected N60 data set. Across 111 reported SPT observations, resistance rises steeply with depth. The median N is 12 at 1-10 m, 23 at 11-14.5 m, and 56 at 15-30 m. The mean values are 12.8, 26.4, and 53.1, respectively. This trend is independently mirrored by the cross-hole velocity profiles discussed below.

All eight original packages also contain CPT/CPTU soundings with cone resistance, sleeve friction, pore pressure, and normalized SBTn plots. The sounding depths range from 11.24 to 14.18 m. Relative to the 18.2-22.2 m pile lengths, this corresponds to only 50.6-70.3% of the pile length, with a mean coverage of approximately 59.6%. The CPT evidence is therefore useful for checking the upper and transitional strata, but it does not sample the toe level of any pile in the present set. The soil-behavior-type classification follows the normalized framework of [3], [16]. The SBTn panels are dominated by clay/clayey-silt and locally organic-like fine-grained classifications in the top profile, with more frequent silty-sand/sandy-silt or sand classifications in the lower half of multiple soundings. Because the project records mostly give these CPT results as graphs rather than exportable digital data, we read them qualitatively and do not reverse-digitize qc or fs for capacity calculations.

2.4 Cross-hole seismic

The four independent cross-hole seismic profiles measure compressional-wave velocity (Vp) and shear-wave velocity (Vs) at depths ranging from 1 m to 30 m, and the complete dynamic-property tables include density, Poisson's ratio, dynamic shear modulus (Gd), dynamic Young's modulus (Ed), and bulk modulus. Despite the spatial differences between the four test sites, all four profiles trace a broadly similar depth-dependent structure.

The combined mean Vs is 217 m/s at 1-10 m, 331 m/s at 11-14 m, and 517 m/s at 15-30 m. The dynamic moduli follow the same pattern, but more sharply: mean Gd rises from around 89 MPa in the top interval to 217 MPa at intermediate depth and 540 MPa below 15 m, whereas mean Ed climbs from approximately 263 MPa to 641 MPa and finally to 1,573 MPa.

Density increases gradually from 1,836 kg/m³ to 1,919 kg/m³ and subsequently to 1,984 kg/m³ at similar depths. The rise in dynamic stiffness therefore comes mainly from the increase in Vs; the change in density is small by comparison (Figure 1).

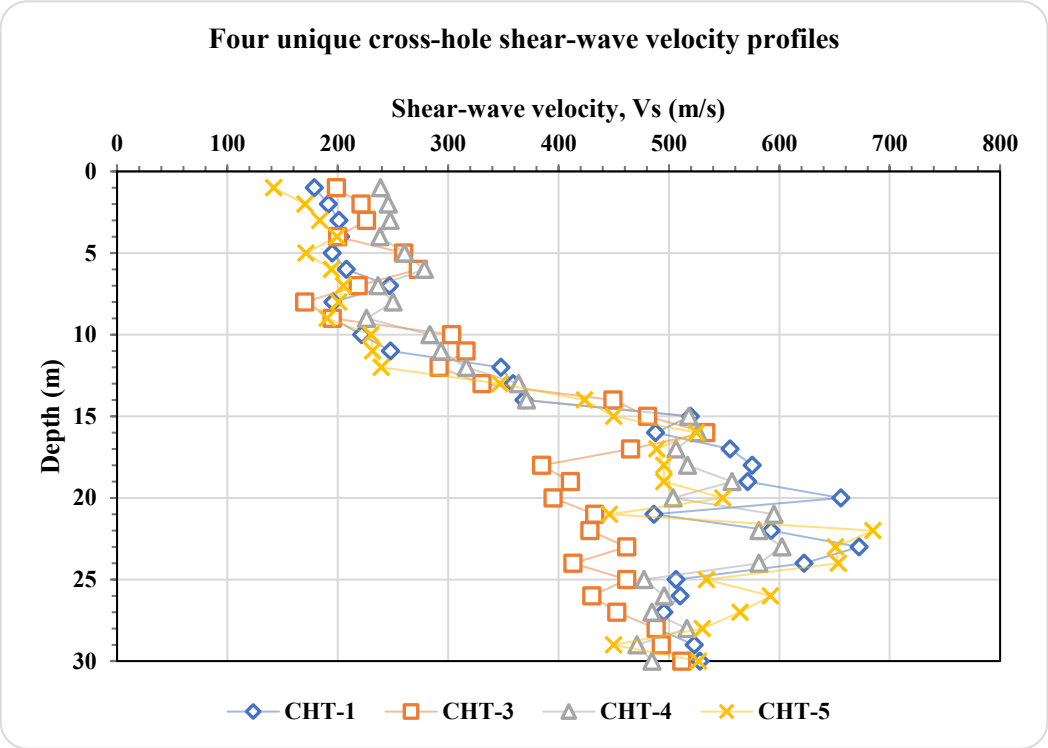


Figure 1 Four unique cross-hole shear-wave velocity profiles recovered from the original TP source packages. CHT-1 is added from TP-8; duplicated profiles appearing in more than one package are plotted once.

Table 3 Depth-banded integration of reported SPT and cross-hole evidence. Asterisks denote seismic statistics calculated over 11-14 m because the seismic sampling grid is at integer depths.

Depth band	SPT n	Median N (range)	Mean vs. m/s (range)	Mean Gd (MPa)	Mean Ed (MPa)	Integrated interpretation
1-10 m	40	12 (5-28)	217 (142-303)	89	263	Shallow fine-grained sequence; low-to-moderate stiffness
11-14.5 m	23	23 (11-44)	331 (232-449)	217	641	Transition interval: rapidly increasing penetration resistance and stiffness
15-30 m	48	56 (20-86)	517 (385-685)	540	1573	Deep stiff/dense sequence; all profiles exceed about 500 m/s by 15-16 m.

The depth of the first exceedance of Vs = 500 m/s is 15 m at CHT-1, 16 m at CHT-3, 15 m at CHT-4, and 16 m at CHT-5. The cross-profile mean Vs rises from approximately 350 m/s at 13 m to 403 m/s at 14 m, 492 m/s at 15 m, and 518 m/s at 16 m. This 13-16 m interval is therefore the most reproducible stiffness transition in the original dataset. It lies close to or slightly below the termination of the CPT/CPTU soundings and well above the toes of the 18.2-22.2 m piles.

2.5 Static axial load test

The compiled pile load test records identify an ASTM D1143 standard loading procedure (ASTM International, 2020; Dhi-Qar Combined Cycle Power Plant, 2017). TP-1 to TP-8 form the primary comparison set. TP-1 and TP-6 were tested to 1620 kN, equal to 200% of their 810 kN service load. TP-2, TP-3, TP-4, TP-5, TP-7, and TP-8 were tested to 2900 kN, equal to 200% of their 1450 kN service load. One further record, TP-A in the

worksheet, has a two-cycle test, the second cycle reaching 4350 kN (300% of the 1450 kN service load). Its borehole, coordinates, and pile geometry are not described in the source packages, therefore it cannot be linked to a characterization package and is removed from any pile-level analyses in this study; it is shown in Table 4 solely as an indicator of reaction at a higher load level. The maximum measured settlements remain small relative to the 800 mm pile diameter, therefore the field tests are understood primarily as high-level proof/serviceability evidence rather than direct failure testing. Plate 2 illustrates the reaction/loading configuration utilized for the static axial compression testing.



Plate 2 At the project site, a static axial compression pile-loading test was carried out utilizing a kentledge loading platform and concrete block reaction masses.

Table 4 Summary of measured static pile-load response from the compiled project records (Dhi-Qar Combined Cycle Power Plant, 2017).

Pile/cycle	Service load (kN)	Max test load (kN)	Net settlement at max (mm)	Residual (mm)	Max settlement/D (%)
TP-1	810	1620	2.50	0.62	0.31
TP-2	1450	2900	3.60	0.92	0.45
TP-3	1450	2900	6.81	1.92	0.85
TP-4	1450	2900	5.91	1.66	0.74
TP-5	1450	2900	6.54	1.81	0.82
TP-6	810	1620	7.53	1.52	0.94
TP-7	1450	2900	5.27	0.71	0.66
TP-8	1450	2900	4.48	0.83	0.56
TP-A cycle 1	1450	2900	4.68	0.96	0.59
TP-A cycle 2	1450	4350	7.01	0.98	0.88

3. Analytical and Cross-Checking Methodology

3.1 Source reconciliation and evidence hierarchy

The borehole identity, coordinates, groundwater level, laboratory values, SPT values, CPT/CPTU identity and depth, and cross-hole tables were all based on the original TP1-TP8 PDF files. We reviewed the original source if there was a difference in coverage between the original packages and the created workbook. TP-8 is the most obvious example: its package includes BH01, a full SPT profile, CPT-1, and CHT-1. As a result, TP-8 is regarded as a fully described pile rather than simply an interpreted one.

Duplicated seismic tables were found by comparing the whole depth-by-depth Vp/Vs sequence. For pooled seismic data, each distinct profile was tallied once. For the SPT-Vs consistency analysis, one borehole was assigned to each unique complete cross-hole dataset: BH01/CHT-1, BH15/CHT-3, BH22/CHT-4, and BH51/CHT-5.

3.2 Laboratory strength versus penetration-implied strength screening

An explicit strength cross-check is included since it answers a different query than the depth-matched penetration-seismic correlation. Laboratory strength was compared to the strength implied by the project-adopted Stroud-type conversion of 4.5 kPa per reported blow count for four piles with laboratory undrained-strength summaries and the corresponding penetration dataset used in the original design workflow [17], [18], [19]. Because hammer energy, rod length, sampler, and borehole correction metadata are unavailable, the reported blow counts are not relabeled as rigorously corrected values. The comparison is therefore used only as a screening test of internal consistency, not as a new strength correlation.

The screening readings are compared on a typical pile scale rather than as depth-exact measurements. Laboratory undrained strengths are derived from the reported unconfined or unconsolidated-undrained tests, whereas the penetration route reflects in-situ mass behavior and inherits the uncertainty of the empirical transformation. A large systematic difference is interpreted as evidence that the two routes should not be mixed in a capacity model without reconciliation.

3.3 Small-strain stiffness versus strength screening

The second cross-check evaluates whether cross-hole seismic stiffness can be interpreted at the same strain level as pile-capacity strength parameters. Maximum small-strain shear modulus is obtained from density and shear-wave velocity. Dividing this modulus by laboratory undrained strength produces an apparent rigidity ratio; however, the ratio is not interpreted as an operational pile-design rigidity index because the seismic modulus is mobilized at strains many orders of magnitude smaller than those associated with shaft and base resistance. Published modulus-reduction frameworks show that stiffness decreases strongly with increasing strain and that the reduction is influenced by plasticity and stress history [2], [8], [20].

Accordingly, this calculation is used as a diagnostic of strain-scale incompatibility. Its purpose is to demonstrate why a physically correct seismic measurement can become misleading if inserted directly into a capacity relationship calibrated at much larger strains.

3.4 Depth reconciliation of laboratory and in-situ evidence

Laboratory sample intervals were interpreted at their reported depths without interpolation of missing strength data. SPT values were retained at the test depth shown on each borehole log. Depth-band statistics were calculated directly from the 111 reported SPT N-values across the eight boreholes. CPT/CPTU depths, coordinates, and SBTn classifications were taken from the source plots. No attempt was made to digitize graphical qc or fs curves because that would add an unquantified digitization error; accordingly, CPT is used as qualitative stratigraphic corroboration in the present paper rather than as an independent numerical capacity method.

3.5 Seismic elastic parameters and strain-scale interpretation

The source reports provide density and dynamic moduli directly. Their internal consistency is represented by the standard small-strain relationships given in Eqs. (1)-(3):

$$G_{max} = \rho V_s^2 \tag{1}$$

$$v = \left(V_p^2 - 2V_s^2\right)/\left[2\left(V_p^2 - V_s^2\right)\right] \tag{2}$$

$$E_{dyn} = 2G_{max}(1 + v) \tag{3}$$

These quantities are retained to describe relative stiffness architecture, transition depths, and cross-source consistency.

3.6 SPT-seismic consistency analysis

At each SPT depth in the four selected borehole-cross-hole pairs, Vs was obtained by linear interpolation between the 1 m cross-hole measurement levels. This gives 59 depth-matched observations. Pearson correlation was calculated in the original measurement space. A site-specific power function, $Vs = aN^b$, was fitted by least squares in log-log space and evaluated in the original Vs space using R^2, mean absolute error, and root mean square error. Because the input N-values are uncorrected reported values and the seismic/borehole locations are not proven to be collocated, the regression is treated as an internal consistency tool rather than a transferable design correlation. Two further limits apply to the statistics: the 59 pairs are nested within four profiles, so they are not independent observations and the pooled coefficient and its significance level are reported descriptively; and because N is not corrected to N60 and Vs is not normalized for effective overburden stress, the correlation that survives removal of the depth trend still carries a stress-level component (Figure 2).

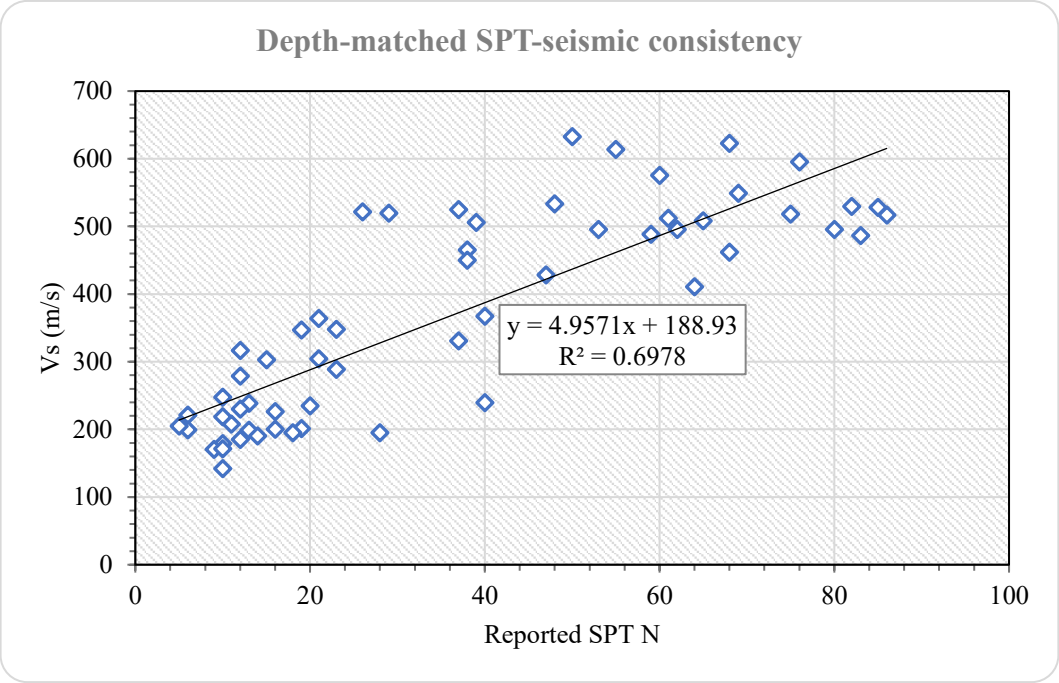


Figure 2 Depth-matched consistency between reported SPT N and cross-hole Vs for four unique borehole-seismic pairs. The fitted relation is project-specific and is not proposed as a universal design correlation.

3.7 Theoretical axial bearing-capacity

The independent static resistance model follows the drilled-shaft framework represented in FHWA GEC-10 and the O'Neill-Reese tradition [21], [22], [23]. The pile is discretized by interpreted geotechnical layer, and total ultimate resistance is given by Eq. (4):

$$Q_{ult} = Q_s + Q_b = \Sigma(q_s \pi D \Delta z) + q_b A_b \quad (4)$$

For clay layers the calculation applies an α-type shaft resistance, $q_s = \alpha\, cu$, with α varying with normalized undrained strength. The source of cu is decisive for everything that follows and is stated explicitly here: the undrained strengths used in the capacity model are laboratory undrained strengths from the undisturbed sample testing program. Because Section 5.5 shows that these two routes differ by a mean factor of 3.06, and because shaft resistance contributes 60.0-77.8% of calculated capacity, the choice of route changes calculated capacity by approximately 50%. Section 5.9 reports the resulting bias for the adopted laboratory route. Substituting the penetration-implied strengths would raise the shaft component, by a factor materially smaller than 3.06, because α falls as normalized undrained strength rises and would drive the mean bias well below unity, so the near-unity bias reported in Section 5.9 is a property of the adopted strength route rather than of the capacity model in general. The alternative route is therefore carried as an explicit sensitivity case so that the parameter inconsistency identified in Section 5.5 and the capacity bias identified in Section 5.9 are not treated as independent findings when they may be two expressions of the same choice. Granular layers are treated using a beta/effective-stress approach. Toe resistance in clay is calculated from the conventional bearing factor of nine after [24], and in granular layers from penetration-resistance-based expressions subject to model caps. The present paper reproduces the compiled model rather than

recalibrating it from the newly recovered CPT plots, because digital CPT traces and construction-specific calibration parameters are not available. The test piles carried no strain gauges or telltales, so the computed division of resistance between shaft and toe is a model output and is not confirmed by measurement.

3.8 Load-test interpretation and comparison metrics

The load-test database contains several extrapolation approaches, including Chin-Kondner (Chin, 1970) , Brinch Hansen, Decourt, De Beer/yield-type interpretation, Mazurkiewicz, and Van der Veen; the assumptions and failure conditions underlying these methods are compared by [25]. Direct displacement criteria such as the Davisson offset (Davisson, 1972) or large-displacement references were generally not reached. Each pile's assembled interpretation set gives several extrapolated capacities, and the lowest of them was adopted as the governing value. This selection rule has three consequences that must be stated. First, the controlling value is not derived from a single, uniform approach: the method that governs it varies from pile to pile, so the Qtest column is a non-homogeneous metric, and part of the variability between piles is attributable to changes of method rather than to subsurface differences. Second, taking a minimum across several estimators biases the retained value downward relative to any one method. Third, at maximum movements of 0.31-0.94% of pile diameter, the load-settlement curves contain very little post-yield curvature, so hyperbolic and graphical asymptotes are poorly conditioned; two piles return a governing value of exactly 4350 kN and one returns 2930 kN against a maximum applied load of 2900 kN, which indicates that these values are constrained by the extent of the test rather than by an identified failure mechanism. The comparison statistics that follow should be read with this in mind. Agreement with the analytical capacity is described using Q_{theory}/Q_{test}, percentage difference, mean bias, mean absolute percentage error, and RMSE. These statistics compare two estimates; they do not imply that the extrapolated field value is an observed ground-truth failure load.

4. Results

4.1 Load-settlement behavior from the static pile load test

Every principal proof test shows low movement relative to pile diameter, though it is worth being precise about which settlement is being reported, since the two quantities used here are not interchangeable. Gross pile-head settlement at maximum load is the total dial-gauge movement at the end of the final load stage, taken from the reprocessed time-settlement records (Table 8); net settlement (Table 4) is that gross value minus whatever was recovered on unloading. Where the two tables disagree by 0.01-0.06 mm, it is because Table 4 came from the summary sheets and Table 8 from the stage-by-stage records; we let the stage records govern. Gross settlement at maximum load ranges from 2.50 mm (TP-1) to 7.53 mm (TP-6), only 0.31-0.94% of the 800 mm pile diameter, and residual movement after unloading runs from about 0.62 to 1.92 mm. So the load-settlement curves show favorable proof-load performance, but they do not show a conventional ultimate failure plateau or a large-displacement mechanism, and Section 5.11 explains why: a large share of this head movement is simply the pile shortening elastically, and that has to be stripped out before the rest is read as ground behavior (Figure 3).

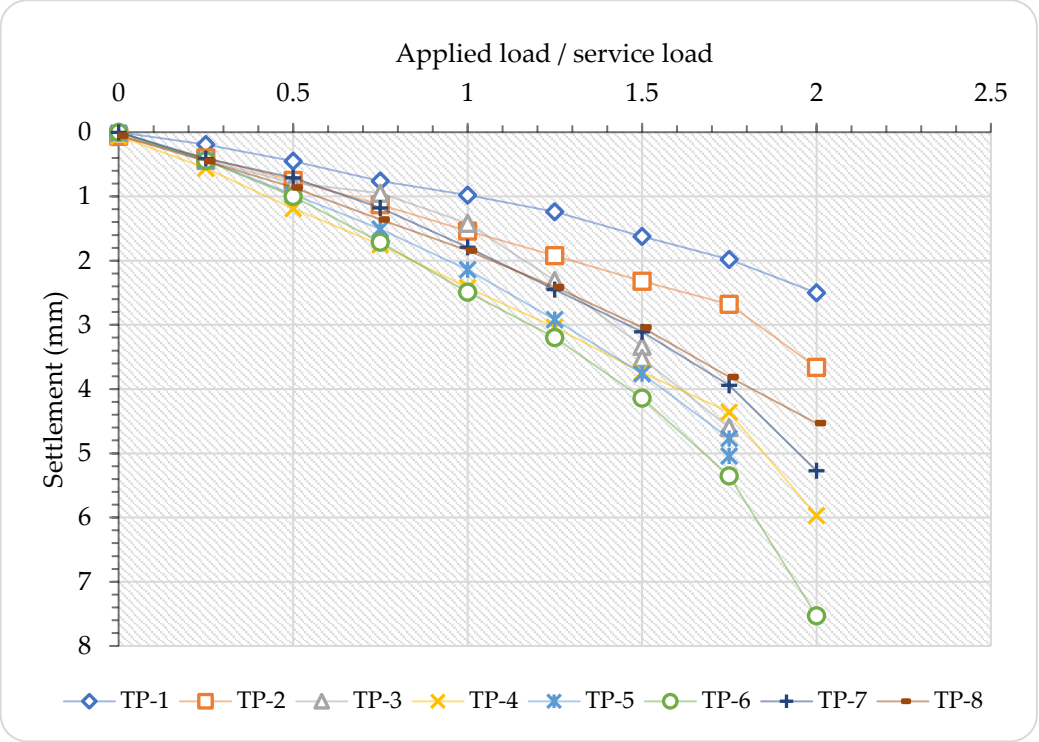


Figure 3 Primary loading response for TP-1 to TP-8 plotted against applied load normalized by service load. Curves are based on the compiled static pile-load-test records.

The pile-by-pile picture is not uniform, though. TP-6 is both the most deformable pile and the one with the lowest analytical ultimate capacity, and that is consistent with its BH32 profile, which shows fairly modest SPT resistance in the lower part of the 18.2 m shaft (N = 21 at 15 m and 42 at 18 m) with stronger resistance only developing below the toe. Although the measured proof-load settlement is not the smallest, TP-5 has the maximum analytical capacity of any pile and strong deep SPT resistance (N = 75-86 through 15-18 m).

This normalized reaction is also consistent with [26], whose 800 mm bored piles settled about 7 mm (nearly 1% of the pile diameter) under a load near 200% of the design value, with none of the tested piles achieving a clear failure condition.

The head settlement of the Dhi-Qar piles at a comparable normalized load was 2.50-7.53 mm, or 0.31-0.94% of the pile diameter D. Pile length and geomaterial are different at the two sites but both lead to the same reading: a stiff pre-failure response at nearly twice the design or service load. An independent field study is a reason to maintain conceptual distinction between extrapolated ultimate resistance and resistance observed during proof testing [15].

4.2 Integrated stratigraphic and soil-layer behavior

The combined borehole, laboratory and in-situ data indicate a site characterized by fine-grained alluvial deposits with some local granular interbeds. The groundwater is shallow at a depth of about 1.60 to 2.40 m below ground, so that most of the pile shaft is below the water table.

Borehole logs through the upper 10 m are dominated by soft to hard silty clays and sandy silty clays with a few organic or salty inclusions. SPT resistance is low across this range, N = 5 to 28, median 12, consistent with the relatively low shear-wave velocities

measured in the cross-hole profiles (pooled Vs 142–303 m/s, mean 217 m/s). Table 2 supports this description and indicates that this shallow fine-grained sequence has medium to high plasticity and variable compressibility.

Drilling and in-situ evidence suggest a transitional sequence rather than one consistent stratum between 11 and 14.5 m. Median SPT resistance increases to N = 23 and pooled mean Vs to about 331 m/s. Several boreholes record clayey, silty sand or sandy clay layers in this interval. The normalized CPT, SBTn profiles are in agreement, showing an increased silty sand and sandy silt classification toward the bottom of the soundings.

All eight CPT/CPTU soundings end in or just above this transitional zone. The CPT data thus describe well the upper and intermediate profile but tell us very little about the conditions at the pile toe. The evidence becomes more internally consistent and stronger below ~15 m, with the median SPT resistance increasing to N = 56, the pooled mean Vs increasing to 517 m/s, and drill descriptions increasingly characterized by very stiff clay, dense sand, and very dense sand. Agreement between soil classification, penetration resistance and small-strain stiffness offers a firmer basis for locating the deep competent zone than any of the three alone.

4.3 Cross-hole seismic stiffness transition

All four seismic profiles show a first order transition with depth. The mean Vs rises from 350 m/s at 13 m to 403 m/s at 14 m and then more steeply to 492 m/s at 15 m and 518 m/s at 16 m.

The velocity (Vs) starts to approach or exceed 500 m/s at 15 m in CHT-1 and CHT-4 and 16 m in CHT-3 and CHT-5. This is a narrow band given the variable alluvial conditions at the site, and indicates that the onset of the deeper competent zone is laterally consistent across the area investigated. The average dynamic shear modulus increases nearly six times from the 1-10 m to the 15-30 m intervals, whereas density increases only about 8%. Thus, the seismic stiffening is a manifestation of a change in the stiffness structure of the soil, not in its density.

The profiles are not the same. The softest is CHT-5 in shallow range (mean Vs close to 189 m/s at 1-10 m), the stiffest is CHT-4 (about 250 m/s). CHT-3 has a lower mean velocity of about 453 m/s, in comparison with CHT-1, CHT-4 and CHT-5 with mean velocities in the deep range of about 526 to 549 m/s. This variability between profiles is important: the site cannot be treated as a single deterministic velocity profile, and local capacity estimates should not be based on a site-wide average Vs.

4.4 SPT-Vs relationship using four unique profiles

By associating each SPT depth with the interpolated Vs from its corresponding unique profile, we obtain 59 depth-matched observations distributed across BH01/CHT-1 (N = 20), BH15/CHT-3 (N = 14), BH22/CHT-4 (N = 11), and BH51/CHT-5 (N = 14). The mean absolute residual is 60.5 m/s, and the root-mean-square error (RMSE) is 76.3 m/s. The pooled Pearson correlation is 0.835 (95% CI 0.74-0.90). A power function fitted by least squares in log-log space gives $V_s = 71.3N^{0.470}$. Correlations for the individual pairs are 0.76 (BH01/CHT-1), 0.88 (BH15/CHT-3), 0.96 (BH22/CHT-4), and 0.86 (BH51/CHT-5). First, the R^2 of 0.739 in the power model is not equivalent to the Pearson coefficient squared ($0.835^2 = 0.698$); the two measure distinct models in distinct spaces. Second, we did not add a smearing adjustment to the log-space back-transformation, thus the fitted curve estimates the median Vs rather than the mean for a given N.

That pooled coefficient is inflated by a confound that must be removed before assigning it a mechanical interpretation. A significant part of the apparent linkage between N

and Vs reflects their common depth trend: both increase strongly with depth (r(N, z) = 0.82 and r(Vs, z) = 0.86 across the 59 pairings). The partial correlation decreases to r = 0.45 when the linear depth trend is removed from both variables and to r = 0.39 when profile means are also removed, leaving within-profile, depth-detrended variation. These values are descriptive, not independent inferential tests: the 59 observations cluster in four boreholes and are vertically autocorrelated at the 1 m seismic sampling interval. A future dataset should use a cluster-aware analysis, such as a mixed-effects model with borehole as a random effect and depth as a fixed covariate.

The scatter itself tells us something. At a given N and depth, Vs still varies because the two measurements respond differently to stress state, fabric, saturation, cementation, and strain level and because the source locations are not proven to be collocated. We treat the regression mainly as an internal consistency benchmark: an observation that deviates markedly from the site-specific relationship is worth checking individually, since it may signal a change in stratigraphy or a data-quality issue. What the regression should not become is a stand-alone transformation from SPT N-value to pile resistance, and its pooled R^2 should not be read as evidence of predictive performance.

4.5 Laboratory strength versus penetration-implied strength

The four piles that were initially included in the strength-screening group had laboratory undrained strengths ranging from 40.8 to 45.8 kPa. However, according to the project's penetration conversion, the actual strengths range from 106.2 to 171.9 kPa, which is 2.40 to 4.21 times greater, with an average of 3.06. Rather than promoting this comparison to a universal corrected-penetration correlation, we are keeping it as a project-design screening calculation because the original reports lack the complete hammer-energy, rod-length, sampler, and borehole correction metadata necessary to build a rigorously corrected SPT dataset. As a bare ratio, the disagreement does not tell us much, because several known biases push in the same direction and can be roughly quantified. The initial stage involves energy correction: the project's conversion is implemented on reported blow counts. However, Stroud's relation is established on N60, and rotary rigs in the region have energy ratios of 45-60%. Consequently, N60 would be 0.75-1.00 times the reported N, resulting in a reduction of the implied strength by up to 25% and a decrease in the mean factor from 3.06 to approximately 2.3. The second point is that the coefficient f_1 is not constant. Stroud demonstrated that it monitors the plasticity index, and the PI range of 18-45%, as reported in Table 2, is encompassed by values of approximately 4.4 to 6 kPa per blow. Consequently, the 4.5 kPa per blow that was implemented in this study is at the low end; the discrepancy is not a result of an unusually high coefficient. Thirdly, the laboratory values are primarily derived from unconfined compression tests, which may underestimate undrained strength due to sampling disturbance and the absence of confinement (DeGroot et al., 2005, discuss the sampling and testing controls required to assess this condition). Fourth and most challenging to determine, the two routes encompass distinct depth intervals. The representative penetration values in Table 3 are averaged across the entire characterized profile, whereas the undisturbed strength data are concentrated in the upper 10 m. Consequently, a portion of the ratio is a comparison between stiffer deep material and shallower samples. The combined effects of the first three yield about 50% of the measured factor of 3.06; the remaining 1.5-2 must be explained in a site-specific manner and the most likely candidate is a depth-support mismatch. None of these change the design implication; if anything they strengthen it; the two parameter routes cannot be mixed within one layer-based model without first working out which of these effects apply [17], [18], [19].

The design takeaway is really about internal consistency, i.e., laboratory- and penetration-derived strengths should not be mixed in a layer-based shaft-resistance model

unless we can explain why the two routes diverge systematically. This screening does not determine which route is "correct" in general; it merely indicates that the disagreement is large enough to materially alter the calculated shaft resistance (Figure 4).

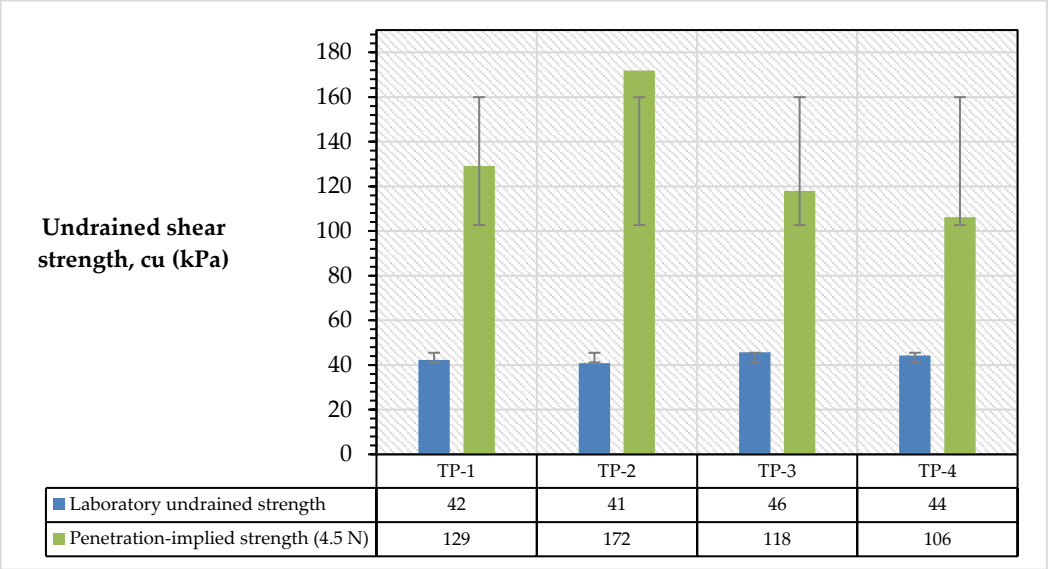


Figure 4 Laboratory undrained strength versus the project penetration-implied strength for the four-pile screening subset. The penetration route gives values approximately two to four times higher at every pile.

4.6 Small-strain seismic stiffness versus laboratory strength

After removing duplicates, the small-strain stiffness screening is performed using the unique full cross-hole profiles of TP-1, TP-2, TP-5 and TP-8. Apparent ratios of about 6,083-6,842 were achieved by taking the ratio of the maximum small strain shear modulus representative of the shaft to the representative laboratory undrained strength. These ratios are more than an order of magnitude higher than the operational rigidity index ranges commonly used in cavity-expansion and pile-deformation frameworks [8], [20], [26], [27], [28], [29].

Two phenomena are involved here, and the second limits the extent to which we can extend the interpretation. The first is the strain regime: near-elastic stiffness is measured in cross-hole seismic testing at strains of ~10^{-6}, whereas shaft and toe resistance mobilize at strains three to four orders of magnitude larger, so a ratio of this magnitude is expected by definition and is not a finding in itself. The second is depth support; the shaft-representative velocities of 355-409 m/s reflect stiff to very stiff material in the middle and lower profile, but the representative laboratory strengths of 40.8-48.8 kPa come from undisturbed samples concentrated in the upper 10 m. Numerator and denominator are therefore not describing the same soil, and that mismatch inflates the ratio on top of the strain-scale difference. We keep this calculation only as a diagnostic that the two quantities cannot be swapped for one another; it is not a rigidity index, it feeds into no capacity calculation, and no value in Table 5 should be carried into design. To attribute the residual difference solely to strain scale, a depth matched comparison over a common interval is required, which is unsupported by this dataset.

TP-8 is paired with CHT-1, the profile specific to its own source package; TP-4 is taken out of this screening as its seismic tables are duplicates of CHT-3 and CHT-5.

For TP-8, the unique cross-hole profile gives a shaft-representative mean shear-wave velocity of about 355 m/s and a mean maximum small-strain shear modulus of about 295 MPa; paired with a representative laboratory undrained strength of about 46.7 kPa, that

works out to an apparent ratio of about 6,329. Using only the unique profile avoids the pseudo-replication introduced by a duplicated seismic profile, and it does not change the strain-scale conclusion (Figure 5).

Table 5 Apparent small-strain stiffness-to-strength ratios after reconciliation of the unique full cross-hole profiles.

Pile	Mean shear-wave velocity (m/s)	Mean maximum small-strain shear modulus (MPa)	Representative laboratory undrained strength (kPa)	Apparent modulus/strength ratio	Operational comparison range
TP-1	392	289.7	42.3	6,842	75-500
TP-2	363	248.4	40.8	6,083	75-500
TP-5	409	315.3	48.8	6,457	75-500
TP-8	354.7	295.4	46.7	6,329	75-500

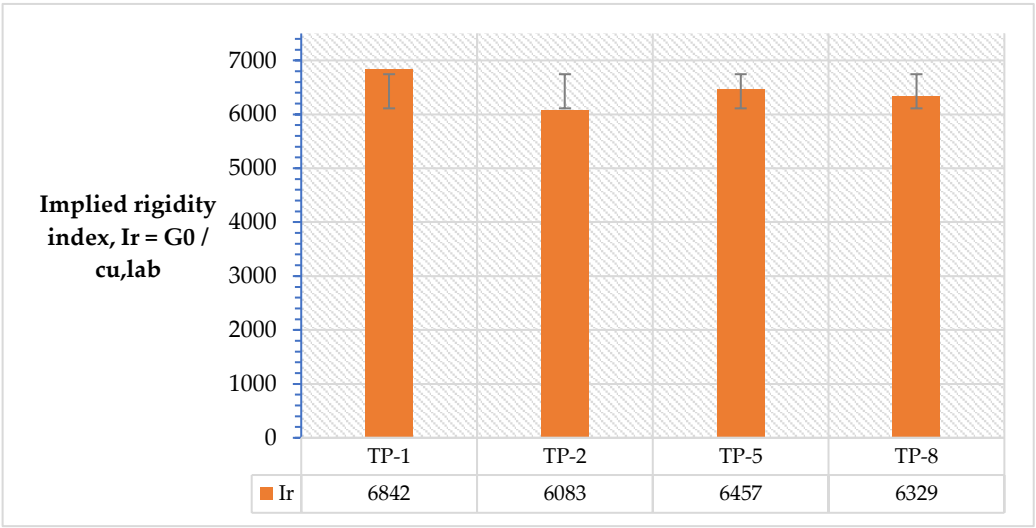


Figure 5 Apparent maximum-small-strain-modulus-to-laboratory-strength ratio for the four unique pile-cross-hole screening pairs. The values are diagnostic of strain-scale incompatibility and are not used as operational design rigidity indices.

4.7 Cone penetration evidence and depth-coverage limitations

Every TP package carries CPT/CPTU evidence, giving a continuous, high-resolution response through the upper 11.24-14.18 m, far denser in depth than the SPT observations. The SBTn profiles independently back up the alternating fine-grained and sandier character already inferred from the boreholes, and in the lower portions of several soundings, they shift toward silty sand/sandy silt, sand, or very stiff categories at roughly the same depth where SPT N and Vs start climbing.

The pile toes, though, sit at 18.2 or 22.2 m, well below where the CPT soundings stop. The CPT depth in the eight piles is only 50.6-70.3% of the pile length. Consequently, any direct toe-resistance calculation based on CPT would require extrapolating beyond the measured sounding depth, which is avoided here. This governs how the different methods are used here. CPT works where it was measured, improving the upper and transitional strata, whereas borehole/SPT and cross-hole data are used for deeper shaft/toe analysis.

4.8 Theoretical shaft and toe resistance

The calculated axial resistance components and relative shaft contributions for TP-1 to TP-8 are summarized in Table 6.

Table 6 Analytical axial resistance and relative shaft contribution calculated on a layer-by-layer basis using the capacity model.

Pile	Q_s (kN)	Q_b (kN)	Q_{ult} (kN)	Shaft share (%)	$Q_{ult}/Q_{service}$
TP-1	2054	1371	3424	60.0	4.23
TP-2	3300	1171	4471	73.8	3.08
TP-3	3081	1140	4221	73.0	2.91
TP-4	2617	746	3363	77.8	2.32
TP-5	3450	1669	5119	67.4	3.53
TP-6	1904	641	2545	74.8	3.14
TP-7	3472	1296	4769	72.8	3.29
TP-8	2974	1458	4432	67.1	3.06

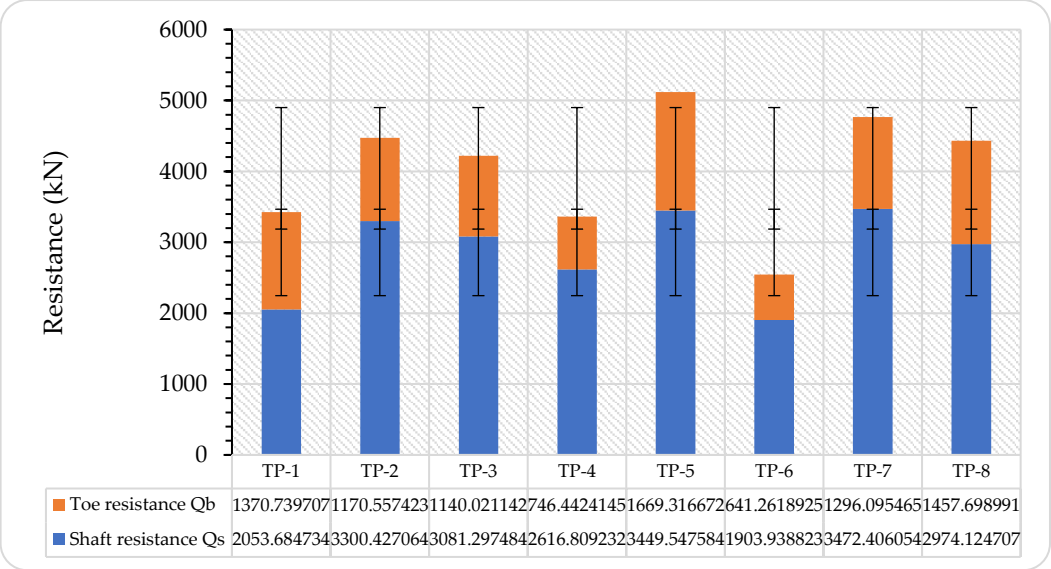


Figure **6** Analytical shaft and toe resistance components for TP-1 to TP-8.

The computed ultimate resistance (Qult) ranges between 2,545 kN (TP-6) and 5,119 kN (TP-5). The shaft resistance dominates each pile's analytical capacity, accounting for 60.0-77.8% of the total (average: 70.8%). This is consistent with piles embedded mainly in clay-rich layers (Figure 6).

The increase in ground stiffness between 15 and 22 m is relevant to the stratigraphic interpretation. This deeper, more competent zone is consistent with greater lower-shaft resistance and toe support in the 18.2-22.2 m piles. However, Vs is not used as a strength or capacity measure; the seismic evidence supports the stratigraphic interpretation that informs, but does not validate, the analytical capacity model.

This shaft dominated response is consistent with the established bored pile mechanisms described by [11], [12], [13], [14]. These studies suggest that shaft resistance can mobilize a substantial proportion of the axial capacity of long bored piles in stratified ground before significant displacement occurs to fully mobilize toe resistance. [15] reported similar behavior, with their 800 mm and 1,200 mm bored piles acting essentially as friction piles since the measured settlements were not large enough to mobilize much end-bearing.

4.9 Comparison of analytical and load-test-derived capacity

The mean bias in reciprocal calibration form (i.e. governing test-derived capacity/theoretical capacity) is 0.90, with a standard deviation of ~0.22, coefficient of variation of 0.25, and mean absolute deviation of ~21.7%.

Table 7 Comparison of analytical and governing load-test-extrapolated axial capacities, with shaft share and the reciprocal test/theory bias.

Pile	Analytical Qult (kN)	Test-derived governing Qu (kN)	Qtheory/Qtest	Difference (%)	Shaft share	Bias, test/theory
TP-1	3424	2673	1.281	+28.1	0.60	0.78
TP-2	4471	4350	1.028	+2.8	0.74	0.97
TP-3	4221	2930	1.441	+44.1	0.73	0.69
TP-4	3363	4350	0.773	−22.7	0.78	1.29
TP-5	5119	3744	1.367	+36.7	0.67	0.73
TP-6	2545	1944	1.309	+30.9	0.75	0.76
TP-7	4769	3780	1.261	+26.1	0.73	0.79
TP-8	4432	5220	0.849	−15.1	0.67	1.18

This reciprocal form is used primarily because it is consistent with the standard resistance-bias convention used in reliability calibration. It is just another way of expressing the same comparison, and is not a separate or statistically independent data set [30]. Figure 7 shows this governing comparison.

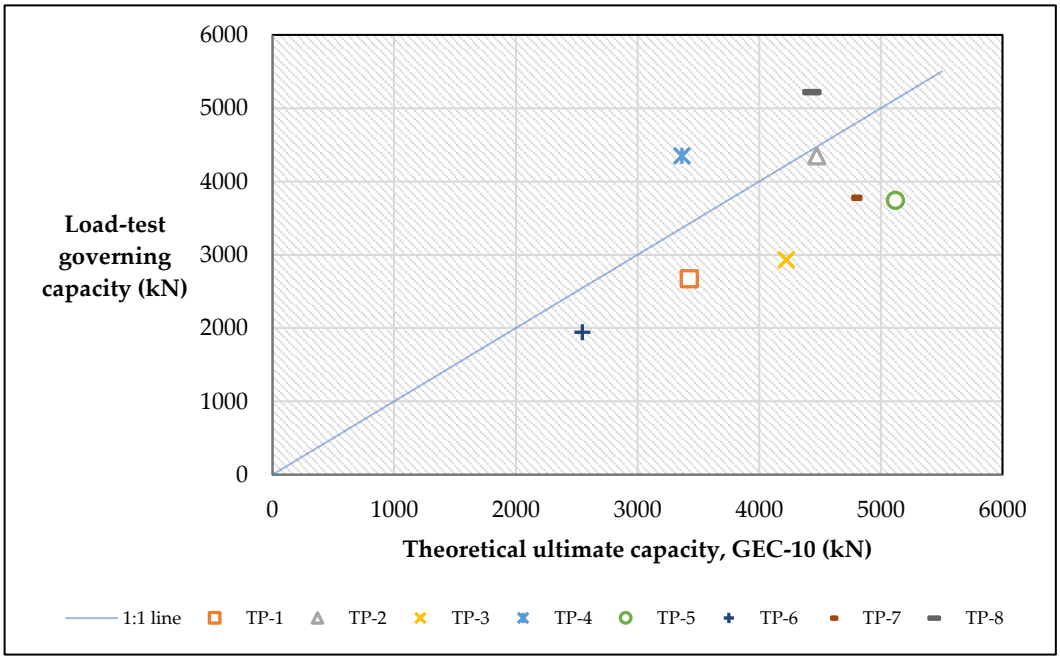


Figure 7 Governing load-test-derived capacity versus theoretical capacity with the one-to-one line. Six of eight piles plot below the line and two above it.

The comparison is not uniformly conservative, nor uniformly unconservative. The Qtheory/Qtest values are in the range 0.773 at TP-4 to 1.441 at TP-3 with a mean of about 1.164. The mean percentage bias is +16.4%, the mean absolute percentage error is of the order of 25.8%, and the RMSE is of the order of 0.9 MN. The best fit is with TP-2. TP-3 and TP-5 are significant overpredictions, and TP-4 and TP-8 are underpredictions of the field extrapolation.

Both extremes merit descriptive examination, but neither establishes a general causal mechanism. TP-3 shows the greatest overprediction (+44.1%). Its deepest 1.7 m of shaft and the entire toe-bearing stratum are extrapolated from the profile above, and BH85 terminates at about 20.5 m beneath a 22.2 m pile. This case is consistent with the risk introduced when the toe stratum is not directly characterized. The 36.7% overprediction of TP-5 may reflect conversion of SPT N-values into strength or resistance parameters in the dense lower zone; construction effects, spatial mismatch, and extrapolation uncertainty cannot be separated with the available records.

The bias ratio's modest correlation ($r = 0.29$) with the analytical shaft-resistance share implies that the pile-to-pile scatter is not accounted for by the 60-78% range in shaft contribution. This matches the reliability literature, in which transformation uncertainty and construction- or site-related variability remain substantial even when the mean bias is near one [9], [30].

An exploratory pile-level examination clarifies why this scatter is to be expected. The mean SPT N-values over the bottom roughly 5 m of each pile correlate strongly with calculated analytical capacity, unsurprising given that the analytical model derives resistance from penetration-based parameters in the first place, but those same N-values have little direct relationship with the settlement measured during proof loading.

This is expected once pile-head movement is understood for what it represents: the overall reaction of the load-transfer system, influenced by shaft and toe mobilization, construction conditions, structural pile compression, and the applied load, rather than merely the N-value near the toe. That is a reason to keep evidence sources genuinely independent and to avoid the circular trap of validating an SPT-based analytical model against another metric drawn from the same SPT data.

The shaft share only changes between 0.60 and 0.78, which limits statistical power and does not account for the capacity dispersion found in this dataset (Figure 8).

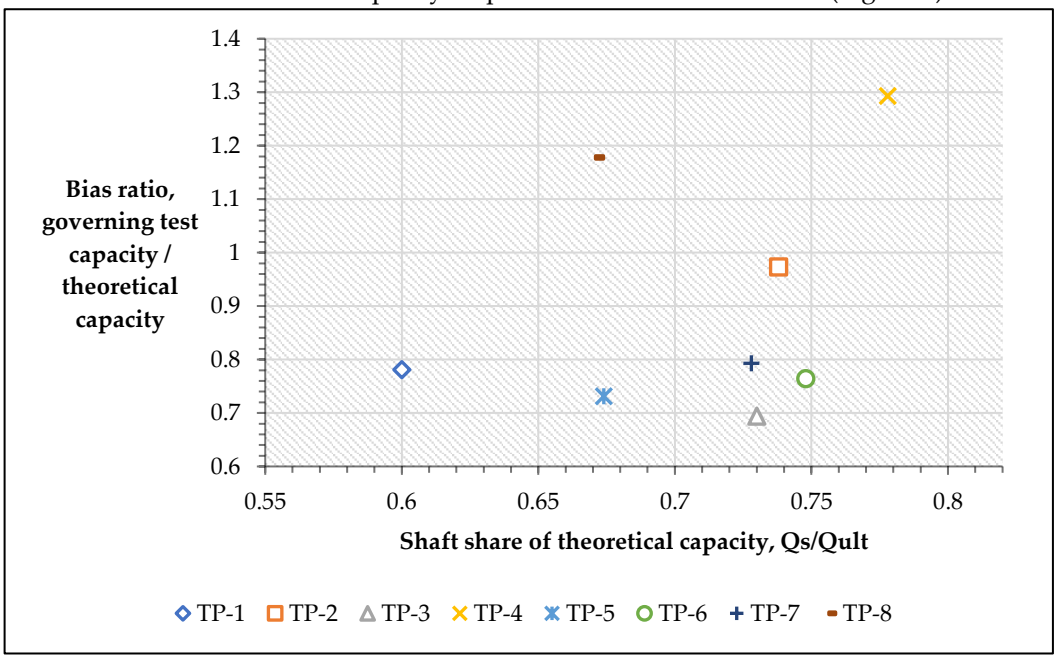


Figure 8 Test-to-theoretical capacity bias versus shaft share of theoretical capacity. No statistically significant relationship is evident within the represented range.

A natural question is whether piles backed by more characterization streams are predicted more accurately. The confirmed data inventory displays three separate evidence streams for TP-1, TP-2, TP-5, and TP-8, compared to two for TP-3, TP-4, TP-6, and TP-7.

Correlating stream count with absolute logarithmic bias gives r = -0.49 across eight piles. This descriptive pattern is too underpowered to support an inference about whether additional characterization streams improve prediction accuracy.

So the interpretation has to stay cautious here. Additional sources of information may well improve the reliability of pile-capacity assessment, but stream count alone cannot prove it; what matters more is systematically integrating each dataset according to its spatial support, applicable strain regime, and reliance on empirical parameter transformations.

4.10 Settlement, recovery, and sustained-load creep

Beyond just comparing ultimate capacities, we reprocessed the stage-by-stage static load-test records to quantify service-load settlement, final proof-load settlement after the 12 h hold, residual settlement after unloading, recovery ratio, and the logarithmic creep slope at proof load. That creep slope is the least-squares gradient of settlement against $\log_{10}$(time) over the interval from 60 min to the end of the 720 min hold (about 1.08 log cycles), and it is strictly a short-duration test parameter, not something extrapolated to service life. Table 8 summarizes these results, Figures 9 and 10 show the time-dependent proof-load response and the relation between proof-load settlement and creep rate.

Table 8 Summary of settlement, residual movement, and proof-load creep metrics derived from the reprocessed stage records.

Pile	Service load (kN)	Service settlement (mm)	Proof settlement (mm)	Residual settlement (mm)	Proof creep slope (mm/log cycle)	Proof creep increment 60 min to end (mm)	Recovery (%)
TP-1	810	0.98	2.5	0.62	0.168	0.23	75.2
TP-2	1450	1.54	3.66	0.98	0.374	0.43	73.2
TP-3	1450	1.42	6.81	1.92	0.439	0.52	71.8
TP-4	1450	2.42	5.97	1.72	0.581	0.66	71.2
TP-5	1450	2.14	6.55	1.82	0.208	0.28	72.2
TP-6	810	2.49	7.53	1.52	0.581	0.65	79.8
TP-7	1450	1.79	5.27	0.71	0.416	0.47	86.5
TP-8	1450	1.84	4.53	0.83	0.232	NA	81.7

Service-load settlements stay very small, and even the 12 h proof-load settlements remain under 1% of pile diameter for every pile. Residual settlements are limited, and recovery ratios are high, so a substantial part of the head movement recovers. TP-6 has the largest absolute proof-load settlement, TP-4 and TP-6 the highest proof-load creep slopes, and TP-7 the strongest rebound after unloading (Figure 9).

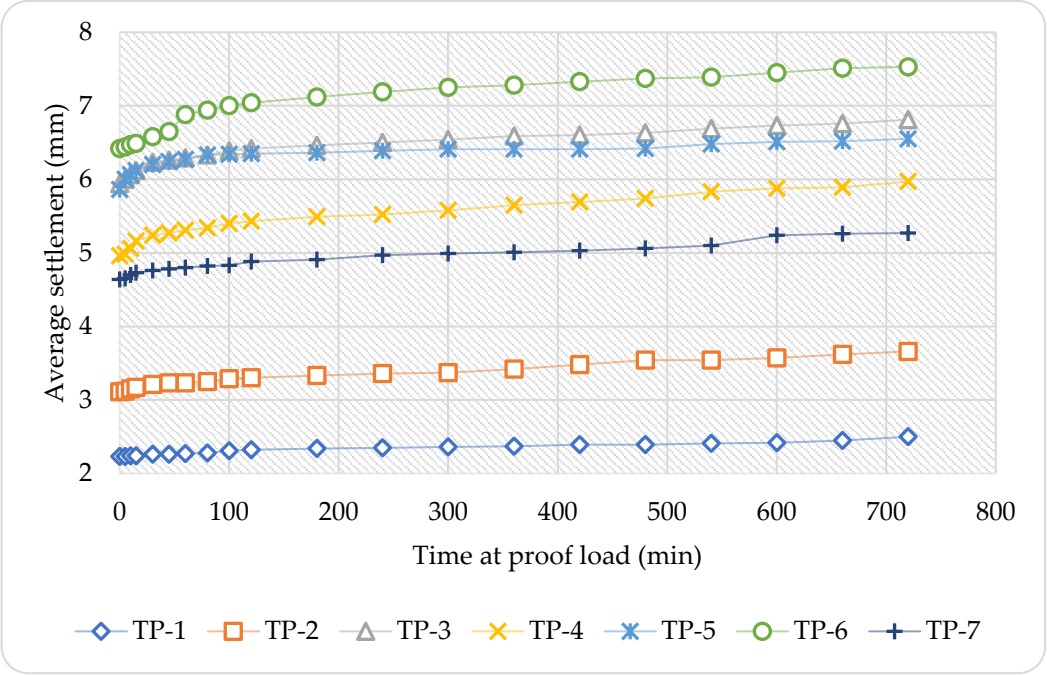


Figure 9 Sustained proof-load time-settlement response, TP-1 to TP-7.

The stage-by-stage time series for TP-8 is not held in the compiled workbook, and TP-8 is therefore not plotted. The creep slope quoted for TP-8 in Table 8 and plotted in Figure 10 was obtained from the summary sheet rather than from a fitted time series; it is not directly comparable with the other seven values and is shown as an open symbol.

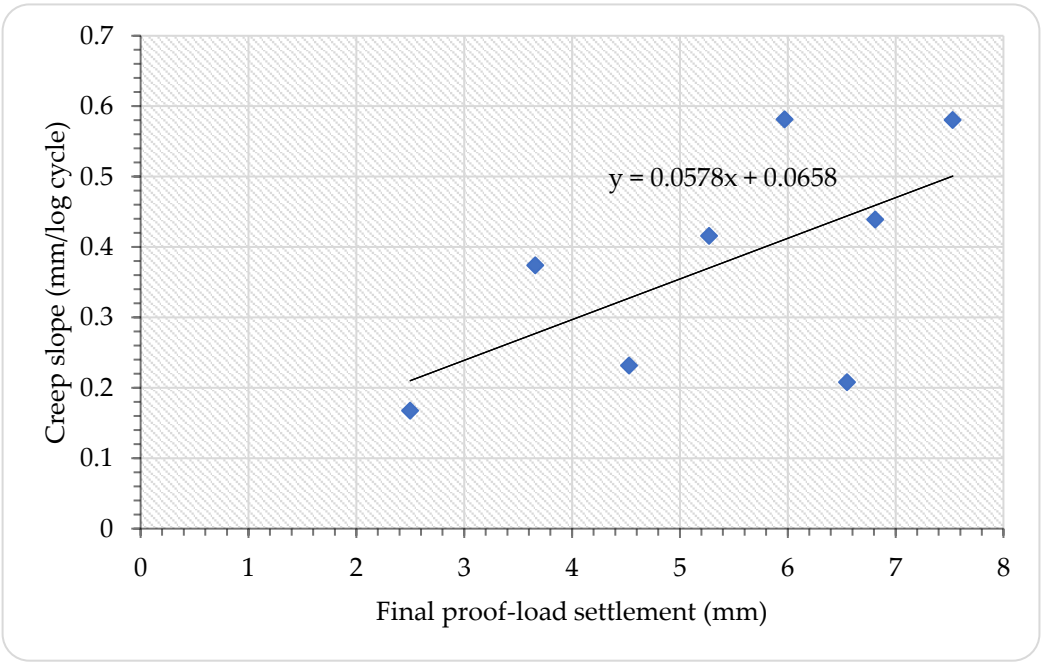


Figure 10 Relationship between final proof-load settlement and proof-load logarithmic creep rate.

The interpreted lower-shaft and toe stratigraphy of each pile can be read directly against its measured serviceability response. TP-1 combines a 10.5-13.5 m clayey/silty-sand interbed with a very stiff sandy silty clay toe zone and shows the smallest movements of the set: 0.98 mm at service load, 2.5 mm at proof load, and the flattest creep slope, 0.168 mm per log cycle. TP-2, whose lower shaft is clay-dominated with a 10.5-16.5 m

clayey silty sand interval above very stiff deep clays, follows at 1.54 and 3.66 mm with a moderate creep slope of 0.374 mm per log cycle. In both piles a granular interbed sits above competent deep clay, and the measured response is correspondingly stiff.

The piles whose lower shafts remain layered or transitional deform more. TP-3 has a thin granular transition near 10.5-12.5 m above stiff to very stiff fat-silty clay, but settles 6.81 mm under the same 1450 kN service load that produces 3.66 mm in TP-2, indicating more deformable lower-shaft or toe behavior than the gross layering suggests. TP-4, with clay and sand lenses alternating in the lower shaft, gives 2.42 mm at service load, 5.97 mm at proof load and the steepest creep slope of the set, 0.581 mm per log cycle. TP-6 settles the most of all, 2.49 and 7.53 mm, and shares that steepest creep slope. The difference lies in the more compressible lower-shaft sequence, not embedment length, as TP-1 has the same 18.2 m length and 810 kN service load but the smallest settlements.

The remaining piles illustrate that proof-load settlement, creep, and rebound need not rank identically. TP-5 has a very dense silty-sand interbed in otherwise stiff to hard clay and the highest analytical capacity of the eight, 5119 kN; its proof-load settlement is still moderately high at 6.55 mm, but the creep increment after 60 min is only 0.28 mm. TP-7 settles 5.27 mm but rebounds 86.5% of that movement. TP-8 is mid-range in service settlement at 1.84 mm with one of the lowest creep slopes at 0.232 mm per log cycle and 81.7% recovery. These pile-level descriptions are compatible with an influence of lower-shaft layering, but the dataset is too small and heterogeneous to establish a general relationship.

Across this small, heterogeneous dataset, the pile-by-pile descriptions are compatible with, but do not demonstrate, a relationship between lower-shaft conditions and serviceability response. Piles with layered transitions or shorter embedment in the identified competent zone, notably TP-4 and TP-6, show larger proof-load settlement and/or creep than several other piles. Differences in pile length, service load, construction conditions, and unmeasured load-transfer behavior prevent causal inference.

4.11 Separation of pile elastic shortening from ground response

Tables 4 and 9 provide settlement values for pile-head motions, which combine the elastic compression of the pile shaft with ground displacement around it. Given the length of these piles relative to the observed movements, that structural component is not a small correction. A shaft with a diameter of 0.8 m has a cross-sectional area of 0.503 m². The secant modulus for the given bored-pile concrete grade is expected to be 25-30 GPa. Two bounding cases are useful here: if the entire applied load reached the toe, compression would be QL/AE; if shaft resistance were instead activated evenly along the shaft, the mean axial force would be roughly half the head load, giving QL/2AE. The real value sits somewhere between these two, and given the shaft-dominated behavior the analytical model points to, it should sit closer to the lower bound.

Table 9 works out both bounds at the maximum applied load for each test. For the 22.2 m piles, the toe-bearing bound is 4.27-5.12 mm and the uniform-transfer bound 2.13-2.56 mm, against measured head movements of 3.66-6.81 mm; for the 18.2 m piles the bounds are 1.96-2.35 mm and 0.98-1.17 mm against 2.50-7.53 mm. As a share of the measured head movement, the uniform-transfer estimate accounts for 13-70% of the total, and for TP-2 the toe-bearing bound actually exceeds the measured movement, which is itself a useful consistency check, since it means load transfer along that shaft has to be substantial. That has three knock-on effects on how other parts of this paper should be read. First, the 71-87% recovery ratios in Table 8 are not a measure of ground rebound: an elastic pile contributing 13-70% of the head movement will recover that portion in full on unloading regardless, so a high recovery ratio is expected even where the ground response only partly recovers. Second, the normalized settlements of 0.31-0.94% D compared against

published values in Section 6.9 are head movements in both datasets, so they are comparable on that basis, but they are not comparable as measures of ground stiffness unless pile length and modulus line up too. Third, the creep slopes in Table 8 are the one quantity this correction does not touch, since concrete creep over a 12 h hold at these stress levels is small, which means the creep measurements are the most directly ground-related piece of serviceability information in the whole dataset.

The practical consequence is that pile-head measurement alone cannot separate shaft from toe mobilization at these displacement levels. Instrumenting future test piles with strain gages or extensometers would resolve that split and turn a proof test into a load-transfer calibration.

Table 9 Calculated pile elastic shortening at maximum applied load, compared with measured pile-head settlement.

Pile	L (m)	Q max (kN)	Measured head settlement (mm)	Elastic shortening, toe-bearing bound (mm)	Elastic shortening, uniform-transfer bound (mm)	Uniform bound as % of measured
TP-1	18.2	1620	2.5	1.96-2.35	0.98-1.17	39-47
TP-2	22.2	2900	3.66	4.27-5.12	2.13-2.56	58-70
TP-3	22.2	2900	6.81	4.27-5.12	2.13-2.56	31-38
TP-4	22.2	2900	5.97	4.27-5.12	2.13-2.56	36-43
TP-5	22.2	2900	6.55	4.27-5.12	2.13-2.56	33-39
TP-6	18.2	1620	7.53	1.96-2.35	0.98-1.17	13-16
TP-7	22.2	2900	5.27	4.27-5.12	2.13-2.56	41-49
TP-8	22.2	2900	4.53	4.27-5.12	2.13-2.56	47-57

4.12 Implication of the measured bias for resistance factor selection

Table 7 provides descriptive bias information: the mean test/theory ratio is 0.90 (95% CI 0.71-1.09 on eight piles) and the coefficient of variation is 0.25. These quantities are not used here to calibrate a design resistance factor. The comparison is based on extrapolated test-derived capacities rather than measured failure resistances, and the sample is too small for a site-specific reliability calibration.

The comparison has three material limitations. First, it uses extrapolated ultimate capacities rather than capacities measured at a defined failure condition. Second, the eight-pile sample cannot establish a stable bias distribution. Third, the apparent dispersion combines subsurface uncertainty with construction effects, spatial mismatch, and variation among extrapolation methods.

A sensitivity calculation can illustrate how strongly any hypothetical resistance factor would depend on assumed dispersion, but it must not be presented as a calibrated design recommendation. Additional full-scale tests taken to a defined failure criterion and analyzed with a consistent interpretation protocol would be required before calibration.

The practical implication is qualitative: a mean bias close to unity does not demonstrate that a design process is reliable when pile-to-pile dispersion remains substantial. Reducing parameter-selection uncertainty and documenting construction conditions are more defensible priorities than modifying a method to force the mean bias toward one.

5. Discussion, Literature Comparison, and Design Implications

5.1 Cross-checking as an explicit design step

The penetration, laboratory, and seismic data are each credible within their respective measurement domains. Cross-checking exposes the systematic two-to-four

discrepancy in inferred strength parameters and confirms that seismic stiffness and capacity-design strength cannot be used interchangeably.

The quality control for the ground model is systematic cross-verification, which identifies where engineering review is needed before a parameter is used in a pile-capacity calculation, whether due to uncertainty in empirical transformation, inconsistent assumptions on strain, sample disturbance, or spatial mismatch [8], [9], [18], [19], [20].

It also matters how the evidence inventory itself is counted. A complete audit of the original TP-1 to TP-8 packages establishes the verified counts of streams per pile, and on that inventory the relationship between stream count and absolute logarithmic bias is moderately negative, but still not statistically significant.

More investigation in itself doesn't help. Additional data improves geotechnical decisions only when the spatial support, strain regime and parameter-transformation assumptions are sufficiently well-matched. This is reflected in the strength-ratio and apparent-rigidity diagnostics: a third measurement stream that disagrees with the other two can uncover a new source of uncertainty while reducing another.

Three evidence streams indicate a common lower-shaft stiffening zone: rapidly increasing SPT N-values, the cross-hole Vs transition reported in Section 5.3, and borehole descriptions of very stiff clay and dense to very dense sand.

The CPTU soundings are not able to directly verify this transition as seven out of eight terminate at or above 13.2 m. Thus, they record the approach to the deeper competent zone, without determining its exact depth or extent. Two caveats are worth noting. SPT resistance, CPTU response and Vs are not mechanically independent. The three respond, to a different degree, to the same underlying soil state, density, stress condition and stiffness structure. Physical grounds therefore predict a shared first-order trend. Second, the convergence of these profiles, which are pooled across a site with borehole-to-CPT separations of 20 to 132 m, supports the view that the transition occurs laterally across the project rather than establishing a single, continuously traceable geological horizon.

This stiffening zone is above the pile toes but within the lower shaft region of each pile tested, with about 7 m of the embedded length below 15 m for the 22.2 m piles and about 3 m for the 18.2 m piles.

This spacing can add significantly to the total axial strength. Analytical calculations indicate a shaft-driven response. As the stiffness and the ground conditions around the shaft improve downwards, the total capacity may be controlled by the shaft long before the toe resistance becomes significant.

However, the deeper Vs values do not agree between profiles and the overall trend has localized reversals, CHT-3 for example, runs lower than the other profiles at many depth levels between 18 and 24 m, while CHT-5 has a distinct high-Vs interval at about 22-24 m. These variations are to be read site-specifically, not averaged into a single universal velocity profile. Cross-hole measurements are well suited to identify depth-dependent stiffness zones and associated uncertainty boundaries in production-pile design. However, the strength characteristics should still be established by rigorous geotechnical testing and calibrated against the observed responses to load tests.

5.2 Cone penetration depth coverage and spatial offset

The source packages reveal both the usefulness and the limitations of the CPT program. Continuous CPT/CPTU traces provide good vertical resolution in the upper 11–14 m where conventional drill sampling is spotty, and SBTn profiles increase confidence in the continuity of shallow layers and help locate sandier transition intervals. However, as there is no sounding that reaches an 18.2 or 22.2 m pile toe, any CPT-based toe resistance at the pile base would be extrapolated rather than measured.

A second constraint is a spatial offset. Borehole-CPT separations are reported from about 20 to 132 m, not an unusual range for a site of this size, but it does mean that a CPT curve should be read as near corroboration rather than an exact stand-in for the borehole at the pile centerline; this is particularly important at TP-6 and TP-7, where the offsets are greatest. In the absence of cross-hole coordinates in the original records, seismic profiles should be regarded as project-scale or local-zone evidence, unless perfect collocation is supported by independent survey data.

5.3 What cross-hole seismic evidence can and cannot support

The cross-hole measurements yield something that traditional strength testing cannot: continuous, depth-resolved small-strain stiffness beyond the pile toe. The four profiles reach 30 m against the approximately 14 m ceiling of the CPT soundings, making cross-hole testing useful to check if a presumed deep competent zone actually exists below the pile base. It also offers an independent way of detecting sudden stiffness changes that laboratory testing alone may miss.

Direct conversion of shear-wave velocity to pile capacity is not justified. Vs reflects the elastic response of the ground at very small strain, but shaft resistance and toe bearing mobilize at much higher strain levels and depend on parameters that Vs does not reflect: pile-soil interface roughness, stress history, drainage conditions, installation effects, and construction quality.

Accordingly, the SPT-Vs relation is used only as an internal consistency check (Section 5.4), not as a predictive design equation. The R2 suggests a common depth-dependent structure between the datasets but does not support substitution of Vs-derived values for independently calculated geotechnical strength metrics.

5.4 Interpreting proof tests that do not reach failure

The small pile head deflections measured at 200% of the service load are acceptable from a proof test viewpoint since the piles carried the specified verification loads with minimal deflection. This rigid response also limits the estimation of ultimate capacity, as the obtained load-settlement curves display little post-yield curvature.

This is a distinction that matters when comparing analytical predictions with capacity derived from field testing. The mean absolute difference of 25.8% between two estimated capacities is not an error against a known capacity but a combination of analytical model, extrapolation method, spatial ground variability and construction effects that is not clearly captured by either computation.

5.5 Pile-specific consistency and divergence

The individual piles show why the sources must be read together. TP-6 has the lowest analytical capacity and greatest normalized proof-load settlement, consistent with its lower-shaft profile: SPT resistance is low between 15 and 18 m and high below 18.2 m, so calculated strength and observed deformation are in the same direction. TP-2 is however a good local calibration reference because it has the best correlation between analytical and test capacity ($Q_{theory}/Q_{test} = 1.03$).

TP-5 diverges from the simple pattern. BH22 has very high SPT values in the deep range where the analytical model gives the largest Q_{ult} of the eight piles. However, TP-5 does not have the smallest proof-load settlement and its controlling test extrapolation is much lower than the analytical prediction. The difference may be due to spatial mismatch, structural effects, shaft/toe mobilization, construction conditions, or ambiguity in the extrapolation process. The defensible conclusion is that a single penetration indicator cannot be used to predict pile performance.

5.6 Regional relevance and practical workflow

This study extends earlier Iraqi cross-hole investigations by incorporating seismic measurements into a comprehensive deep-foundation evaluation methodology [6], [7]. The combined information suggests a four-stage engineering workflow.

First, use borehole data and laboratory soil classifications to determine the site stratigraphy and groundwater conditions. Second, incorporate SPT and CPT/CPTU data to refine the image of in-situ variability and determine transitional depth intervals. Third, employ cross-hole Vs and dynamic-modulus profiles to provide independent evidence of stiffness variation, particularly below the CPT sounding limit. Fourth, use the accepted geotechnical design processes to compute shaft and toe resistance.

5.7 Serviceability implications of settlement and creep

ASTM D1143 concentrates on the load-movement connection from static compression testing, but the reprocessed stage records show that these tests also yield serviceability information, in the movements recorded at the end of each hold period (ASTM International, 2020). For these piles, service-load settlement values are small, and the limited residual movements after unloading suggest the field response is nowhere near a problematic serviceability regime. Proof-load creep slopes stay much smaller than total proof-load settlement, so sustained-load time effects are present but not dominant over the duration of the test.

These results also line up with the broader literature connecting long-term pile behavior to both stratigraphic stiffness contrast and time-dependent clay response [2], [31], [32]. The most meaningful pattern in the Dhi-Qar dataset is not one universal creep value, but how creep and residual movement shift with lower-shaft layering, which argues for a design workflow where static test interpretation is backed up by explicit lower-shaft/toe stratigraphic review, and, where serviceability really matters, by targeted long-duration monitoring or creep-oriented back-analysis rather than capacity estimation alone.

5.8 Material and construction controls not captured by the measured evidence

Two potentially important controls on bored-pile performance are missing from the measured evidence streams, and either may contribute to residual scatter in Table 7.

The borehole descriptions and laboratory summaries both contain chemical indicators, and the upper profile contains salt-bearing and locally organic traces. However, the available analysis does not quantify sulfate exposure, groundwater chemistry, or pile concrete durability class. The short-term proof tests therefore say nothing about chemical durability or long-term shaft-interface degradation. Before this capacity comparison is used in a long-term design context, the chemical results should be reported and checked against the project's own durability requirements.

The second is construction. Shaft resistance in bored piles is governed by excavation support, standing time, base cleanliness, and concrete placement at least as much as by the ground parameters that go into a capacity model, yet the support fluid used, the time between excavation and concreting, base-cleaning records, and integrity-test results are not in the available records for any of the eight piles. So the analytical model assumes an idealized shaft interface for every pile, while the measured responses come from eight separately constructed shafts. Pile-to-pile construction variability is simply unquantified here, and it is a plausible contributor to the bias coefficient of variation of 0.25 that neither shaft share nor evidence-stream count can explain. Future programs of this kind should treat reporting construction records alongside load-test results as a requirement rather than as optional.

5.9 Comparison with published bored-pile studies

The closest recent field benchmark is [15]. Their El Alamein study and the present Dhi-Qar study have three common features: cast-in-place bored piles with an 800 mm diameter and static proof loading to nearly twice the design/service load, but the ground

conditions differ substantially. The El Alamein piles extended 40-50 m into interbedded geomaterials and weak limestone. The Dhi-Qar piles are much shorter at 18.2-22.2 m, installed mainly in saturated alluvial silty clays with localized silty-sand and clayey-sand layers. So the comparison here is largely a test of whether normalized field behavior holds up across two quite different stratigraphic settings, without assuming that the underlying soil-pile interaction processes are the same. Because the pile length and toe material are different for the two sites, absolute loads and settlements do not carry over; only normalized quantities do. Neither program drove a pile to a defined failure criterion. Both programs verify proof resistance, not measured ultimate capacity. Both are interpreted as shaft-dominated responses. The analytical shaft share here is 60.0-77.8%, and the mean is near 70.8%.

In normalized terms the two datasets agree. [15]reported a displacement of about 1 % D in 800 mm piles at twice the design load. The Dhi-Qar piles, which were shorter and anchored in soil rather than IGM/weak rock, had a low-movement regime of 0.94% D or less. This agrees with the classical observations of [10], [11] that large toe resistance is usually mobilized only with more base movement than most proof tests generate.

A similar pattern is reported by [33], where the analytical capacity of bored piles in granular soil differs from static and dynamic test results without a consistent direction of bias. The comparison between the two studies is limited because the material classes, pile lengths, and design frameworks differ. The analytical-to-test ratio in this study is between 0.77 and 1.44. This does not establish a contradiction; it reinforces the point that prediction bias is site-specific and that load tests address shaft and toe mobilization rather than providing a single universally transferable capacity number.

5.10 Site-specific design implications

At the Dhi-Qar site, the main site-specific outcome is a systematic hierarchy of evidence rather than a new universal pile-capacity equation. When selecting lower-shaft parameters, the independently identified stiffening zone must be represented explicitly; the CPTU soundings corroborate its approach but do not define its full depth. The site-specific Vs-N relationship is an internal validation tool, while static proof tests remain the governing evidence for confirming pile deformation and resistance.

The comparison with [15] further suggests that normalized settlement at approximately twice service/design load is a useful cross-project serviceability indicator. For 800 mm bored piles, settlements on the order of 1% D or less at the proof stage can occur in very different layered geomaterials without direct failure. Nevertheless, this observation should not be converted into an ultimate-capacity criterion; the required toe movement, shaft degradation, construction effects, and long-term creep remain site specific.

5.11 Future data and validation needs

The next research stage should convert this retrospective database into a fully spatial and instrumented calibration dataset. Priority tasks are: (i) recover original cone penetration digital files and compute cone-resistance-, sleeve-friction-, and pore-pressure-based shaft and toe estimates only within measured depth; (ii) recover survey coordinates for the cross-hole arrays; (iii) obtain hammer-energy and standard-penetration correction metadata; (iv) obtain pile concrete modulus, construction logs, base-cleanliness records, and integrity-test results; (v) instrument future load tests to separate shaft and toe mobilization; (vi) digitize complete time-settlement records for all piles and extend sustained-load monitoring; (vii) obtain deeper laboratory compressibility and secondary-compression data; and (viii) use the measured seismic stiffness envelope as a probabilistic stiffness prior rather than as a deterministic strength equation.

6. Conclusions

1. Verified project archive includes eight boreholes, eight cone penetration soundings and four full cross-hole seismic profiles for eight 800 mm cast-in-place piles. Confirmed evidence for analysis is based on removal of duplicate seismic tables and recovery of TP-8 borehole and cross-hole recordings.
2. The individual measurements show a consistent, pronounced transition between 13 and 16 m. By 15-16 m, all four seismic profiles surpass 500 m/s, while median standard penetration resistance climbs from 12 blows in the upper 1-10 m to 56 blows below 15 m. Mean shear-wave velocity rises from 217 to 517 m/s.
3. Although both variables are substantially depth-dependent (r = 0.82 and 0.86 versus depth), fifty-nine depth-matched penetration-seismic observations produce a pooled Pearson correlation value of 0.835. When the shared depth trend is eliminated, partial correlation drops to 0.45 and 0.39 among profiles. The stratigraphic consistency envelope is not a translation from penetration resistance to pile strength or capacity, and the pooled coefficient is not a predictive strength metric.
4. With a mean factor of 3.06, penetration-implied undrained strengths are 2.40-4.21 times comparable laboratory values. Energy correction, plasticity-dependent conversion coefficients, and unconfined-test bias explain for around half of this; the remaining factor of 1.5-2 is likely a depth-support mismatch between shallow undisturbed sample and depth-averaged penetration resistance. The decision between the two paths varies predicted capacity by nearly 50% and must be indicated explicitly in any layer-based model since shaft resistance contributes 60.0-77.8%.
5. The small-strain stiffness screening yields 6,100-6,800 apparent modulus-to-strength ratios. Due to strain regimes and a depth mismatch between seismic and laboratory data, this magnitude is presented as a diagnostic indicating the two values are not interchangeable rather than a site attribute.
6. High-resolution cone penetration testing confirms the upper and transitional profile but ends at 11.24-14.18 m, 50.6-70.3% pile length. Extrapolating it to toe resistance without additional data is therefore not supported.
7. Maximum pile-head settlement is 2.50-7.53 mm, or 0.31-0.94% of pile diameter, with low residual movement and mild short-term creep in static proof tests to twice service load. The recovery ratios of 71-87% are not a measure of ground rebound because calculated pile elastic shortening accounts for 13-70% of that head movement. The creep slopes are the most directly ground-related serviceability information from these tests.
8. The analytical model predicts axial resistance of 2.55-5.12 MN and shaft dominance of 60.0-77.8%.
9. The analysis-to-test ratio of 0.77 to 1.44 shows substantial scatter between analytical and test-derived capacities. No resistance factor is recommended from this dataset: the eight-pile sample and extrapolated test capacities are insufficient for calibration. A mean bias close to unity therefore does not establish a well-calibrated design method.
10. With eight piles, the number of verified evidence streams cannot support an inference about prediction error. The negative descriptive correlation (r = -0.49) has a wide uncertainty range at this sample size. The data coverage shows the largest analytical

overprediction for the borehole-ending-above-the-toe pile. This is an observation on data provenance and investigation depth, not evidence that further site characterization improves prediction.

11. The most defensible configuration is hierarchical workflow. Laboratory testing provides index properties, strength and compressibility; penetration testing provides in-situ resistance and stratigraphic variability; cross-hole seismic testing provides independent stiffness continuity and deeper transitions; layer-based analyses provide shaft and toe resistance; and static load testing provides deformation, rebound, creep and field resistance. Disagreements across evidence streams are diagnostic results that require engineering explanations, not noise.

Author Contributions: Investigation, A.A.; Methodology, K.A.-K.; Visualization, A.Y.; Writing—original draft preparation, A.J.; Supervision and Writing—review and editing, A.A.R.; Validation, H.A. All authors have read and agreed to the published version of the manuscript.

Funding: This research received no external funding.

Data Availability Statement: [AUTHOR CONFIRM: State whether the third-party project records, derived datasets, and calculation workbook can be made available; identify the data owner, access route, and any permission or confidentiality restriction.]

Informed Consent Statement: [AUTHOR CONFIRM: Use 'Not applicable' only if no human participants or identifiable human data were involved.]

Institutional Review Board Statement: [AUTHOR CONFIRM: Use 'Not applicable' only if no human participants, human data, or human material were involved.]

Acknowledgments: The authors acknowledge the General Company of Electrical Energy Distribution, Southern Region, Ministry of Electricity, Iraq, for support.

Conflicts of Interest: The authors declare no conflicts of interest. The study received no external funding; therefore, no funder had any role in the design of the study; the collection, analysis, or interpretation of data; the writing of the manuscript; or the decision to publish the results.

Notation and Abbreviations

Symbol / abbreviation	Definition as used in this paper	Unit
SPT	Standard penetration test	–
N, N60	SPT blow count; N60 is the energy-corrected blow count	blows / 300 mm
CPT	Cone penetration test	–
CPTU	Piezocone penetration test (with pore-pressure measurement)	–
qc	Cone tip resistance	MPa
fs	Cone sleeve friction	kPa
CHT	Cross-hole seismic test profile (CHT-1, CHT-3, CHT-4, CHT-5)	–
BH	Borehole	–
TP	Test pile (TP-1 to TP-8)	–
GWT	Groundwater table depth	m
IGM	Intermediate geomaterial	–
Vp	Compressional-wave velocity	m/s
Vs	Shear-wave velocity	m/s
Gd	Dynamic shear modulus from cross-hole measurement	MPa
Gmax	Maximum small-strain shear modulus, $G_{max} = \rho V_s^2$	MPa
Ed	Dynamic Young's modulus from cross-hole measurement	MPa
ρ	Soil mass density	Mg/m^3
ν	Poisson's ratio	dimensionless
cu (su)	Undrained shear strength	kPa
z, Δz	Depth below ground level; layer thickness increment in the discretized capacity model	m
D	Pile diameter (0.8 m for the piles compared here)	m
L	Embedded pile length	m
A, Ab	Pile shaft cross-sectional area; pile toe (base) area	m^2
E	Elastic modulus of the pile concrete	GPa
qs, qb	Unit shaft resistance; unit toe resistance	kPa
α	Adhesion factor in the alpha-type shaft resistance, $q_s = \alpha\, cu$	dimensionless
β	Effective-stress shaft-resistance coefficient in granular layers; also the reliability index where LRFD calibration is discussed	dimensionless
Q	Applied pile-head load	kN
Qs, Qb	Ultimate shaft resistance; ultimate toe resistance	kN
Qult	Total ultimate axial resistance, $Q_{ult} = Q_s + Q_b$	kN
Qtheory	Ultimate axial capacity from the analytical static resistance model	kN
Qtest	Ultimate axial capacity derived from the static load test by extrapolation	kN
LRFD	Load and resistance factor design	–
φ	Resistance factor in LRFD	dimensionless
COV	Coefficient of variation	dimensionless
CI	Confidence interval	–
MAPE	Mean absolute percentage error	%
RMSE	Root-mean-square error	units of the fitted variable
ASTM	ASTM International test standard designation	–
FHWA GEC	Federal Highway Administration Geotechnical Engineering Circular	–
NCHRP	National Cooperative Highway Research Program	–

references

[1] ASTM D1143/D1143M, 'Standard Test Methods for Deep Foundation Elements Under Static Axial Compressive Load,' ASTM International, 2020, doi: 10.1520/D1143_D1143M-20.

[2] H. G. Poulos, "Use of shear wave velocity for foundation design," *Geotech. Geol. Eng.*, vol. 40, no. 4, pp. 1921–1938, 2022.

[3] P. K. Robertson, "Soil classification using the cone penetration test," *Can. Geotech. J.*, vol. 27, no. 1, pp. 151–158, 1990.

[4] H. A. Abbas, D. Al-Jeznawi, M. A. Q. Al-Janabi, L. F. A. Bernardo, and M. A. S. C. Jacinto, "Exploring shear wave velocity—N SPT correlations for geotechnical site characterization: a review," *CivilEng*, vol. 5, no. 1, pp. 119–135, 2024.

[5] K. A. M. Nayan, M. R. Taha, N. A. Omar, N. F. Bawadi, S.-H. Joh, and M. N. Omar, "Determination of ultimate pile bearing capacity from a seismic method of shear wave velocity in comparison with conventional methods," *J. Teknol.*, vol. 74, no. 3, pp. 99–102, 2015.

[6] A. N. Alaatabi, A. J. Fakher, M. L. Hussein, R. Ashoor, and H. M. Ali, "Determination of Bearing Capacity of the Soil Using Cross-Hole Seismic Survey for a Water Treatment Plant at Thi Qar Governorate, Southern Iraq," *Iraqi Geol. J.*, pp. 82–93, 2022.

[7] I. M. Jaafer, A. H. Salih, A. A. Laftah, and E. H. Al-Khersan, "Engineering site investigation inside Basrah City, southern Iraq using cross-hole seismic refraction technique (A case study)," *Iraqi Geol. J.*, pp. 52–71, 2024.

[8] F. H. Kulhawy and P. W. Mayne, *Manual on estimating soil properties for foundation design*, vol. 308. Electric Power Research Institute Palo Alto, CA, USA, 1990.

[9] K.-K. Phoon and F. H. Kulhawy, "Characterization of geotechnical variability," *Can. Geotech. J.*, vol. 36, no. 4, pp. 612–624, 1999.

[10] A. S. Vesic, "Design of pile foundations," *NCHRP Synth. Highw. Pract.*, no. 42, 1977.

[11] K. Fleming, A. Weltman, M. Randolph, and K. Elson, *Piling engineering*. CRC press, 2008.

[12] M. Tomlinson and J. Woodward, *Pile design and construction practice*. CRC press, 2007.

[13] M. F. Randolph, "Science and empiricism in pile foundation design," *Géotechnique*, vol. 53, no. 10, pp. 847–875, 2003.

[14] M. W. O'Neill, "Side resistance in piles and drilled shafts," *J. Geotech. geoenvironmental Eng.*, vol. 127, no. 1, pp. 3–16, 2001.

[15] N. Elsakhawy, E. Ibrahim, K. M. Elzahaby, and M. Nabil, "New Design Criteria for Long, Large-Diameter Bored Piles in Near-Shore Interbedded Geomaterials: Insights from Static and Dynamic Test Analysis," *Buildings*, vol. 14, no. 8, Aug. 2024, doi: 10.3390/buildings14082268.

[16] P. K. Robertson, "Interpretation of cone penetration tests—a unified approach," *Can. Geotech. J.*, vol. 46, no. 11, pp. 1337–1355, 2009.

[17] M. A. Stroud, "The standard penetration test in insensitive clays and soft rocks," in *Proceedings of the 1st European Symposium on Penetration Testing, Stockholm, Sweden*, 1974, pp. 367–375.

[18] O. Sivrikaya and E. Toğrol, "Determination of undrained strength of fine-grained soils by means of SPT and its application in Turkey," *Eng. Geol.*, vol. 86, no. 1, pp. 52–69, 2006.

[19] F. White, P. Ingram, and D. Nicholson, "An update of the SPT-cu relationship proposed by M. Stroud in 1974," in *Proceedings of the XVII European conference of soil mechanics geotechnical engineering, Reykjavik*, 2019.

[20] M. Vucetic and R. Dobry, "Effect of soil plasticity on cyclic response," *J. Geotech. Eng.*, vol. 117, no. 1, pp. 89–107, 1991.

[21] D. A. Brown, J. P. Turner, and R. J. Castelli, "Drilled shafts: Construction procedures and LRFD design methods," 2010.

[22] D. A. Brown, J. P. Turner, R. J. Castelli, and E. Loehr, "Drilled shafts: Construction procedures and design methods," 2018.

[23] M. W. O'Neil and L. C. Reese, "Drilled shafts: Construction procedures and design methods," 1999.

[24] A. W. Skempton, 'The Bearing Capacity of Clays,' in Proceedings of the Building Research Congress, London, UK, 1951, vol. 1, pp. 180-189.

[25] B. Fellenius, *Basics of foundation design*. Lulu. com, 2017.

[26] J. M. Keaveny and J. K. Mitchell, "Strength of fine-grained soils using the piezocone," *Publ. Geotek. Inst.*, no. 171, pp. 1–9, 1988.

[27] P. W. Mayne and F. S. Niazi, "Evaluating axial elastic pile response from cone penetration tests (The 2009 Michael W. O'Neill Lecture)," *DFI Journal-The J. Deep Found. Inst.*, vol. 3, no. 1, pp. 3–12, 2009.

[28] M. F. Randolph and C. P. Wroth, "Analysis of deformation of vertically loaded piles," *J. Geotech. Eng. Div.*, vol. 104, no. 12, pp. 1465–1488, 1978.

[29] A. S. Vesić, "Expansion of cavities in infinite soil mass," *J. soil Mech. Found. Div.*, vol. 98, no. 3, pp. 265–290, 1972.

[30] S. G. Paikowsky, *Load and resistance factor design (LRFD) for deep foundations*, vol. 507. Transportation Research Board, 2004.

[31] L. Li, W. Gong, and J. Li, "Effects of clay creep on long-term load-carrying behaviors of bored piles: Aiming at reusing existing bored piles," *Int. J. Geomech.*, vol. 20, no. 8, p. 4020132, 2020.

[32] Q. Wang, J. Li, T. Fang, and S. Yu, "Database analysis of long-term settlement behavior of pile foundations in Shanghai soft coastal clays," *Buildings*, vol. 14, no. 11, p. 3334, 2024.

[33] A. Kurniawandy, V. H. Parulian, A. Ridwan, and Y. Inanda, "Analisis Empiris Penurunan dan Daya Dukung Batas dengan Metode Static Loading Test (SLT)," *J. Teknol. dan Rekayasa Sipil*, vol. 4, no. 1, pp. 1–9, 2025.